Author/s:
Tidu, F;De Zuani, M;Jose, SS;Bendíčková, K;Kubala, L;Caruso, F;Cavalieri, F;Forte, G;Frič, J

Title:
NFAT signaling in human mesenchymal stromal cells affects extracellular matrix remodeling and antifungal immune responses

Date:
2021-06-25

Citation:
Tidu, F., De Zuani, M., Jose, S. S., Bendíčková, K., Kubala, L., Caruso, F., Cavalieri, F., Forte, G. & Frič, J. (2021). NFAT signaling in human mesenchymal stromal cells affects extracellular matrix remodeling and antifungal immune responses. Iscience, 24 (6), https://doi.org/10.1016/j.isci.2021.102683.

Persistent Link:
https://hdl.handle.net/11343/276488

iScience

CellPress
OPEN ACCESS

Article

# NFAT signaling in human mesenchymal stromal cells affects extracellular matrix remodeling and antifungal immune responses

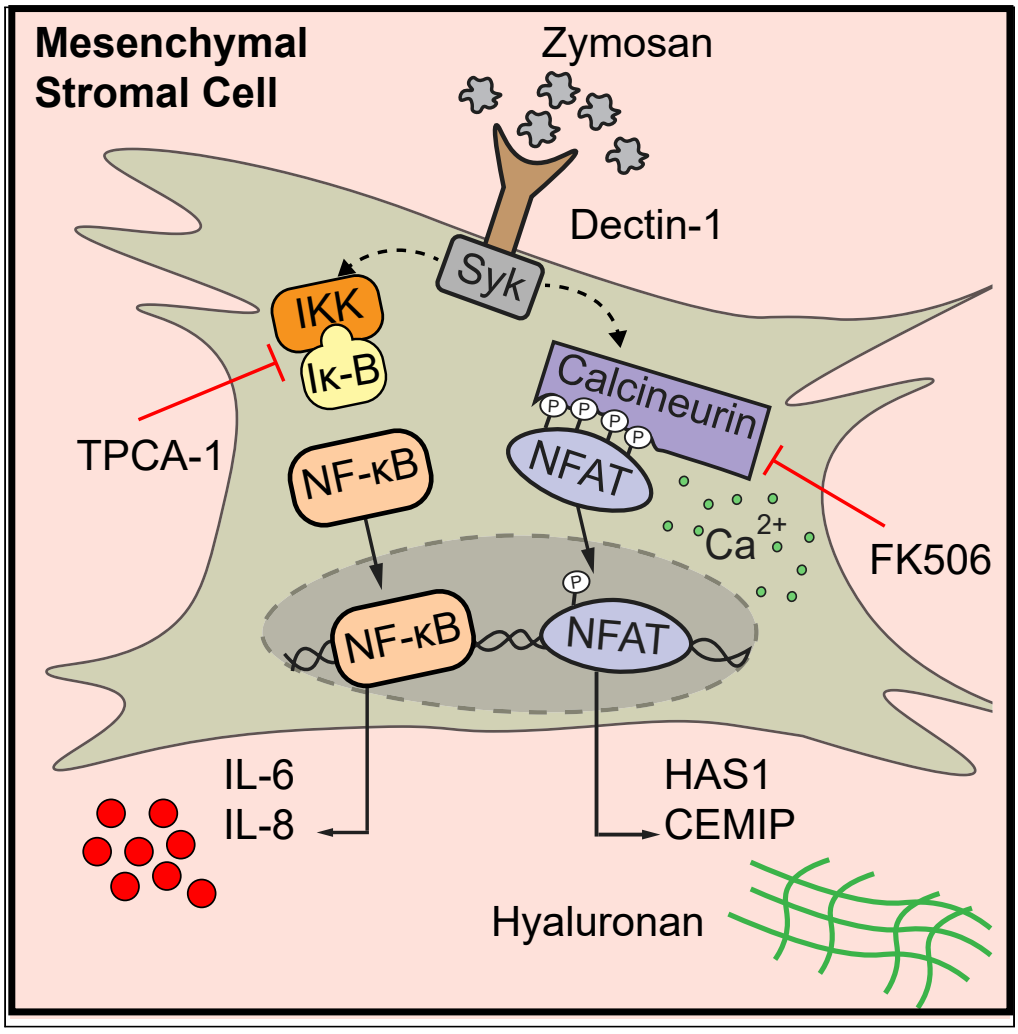


Federico Tidu, Marco De Zuani, Shyam Sushama Jose, ..., Francesca Cavalieri, Giancarlo Forte, Jan Frič

jan.fric@fnusa.cz

## Highlights

Stimulation of MSCs with zymosan activates NFAT and NF-kB via the dectin1-Syk axis

Calcineurin-NFAT inhibition impacts the expression of extracellular matrix genes

NF-kB pathway regulates cytokine expression in zymosan-stimulated MSCs

Selective NFAT inhibition in MSCs impacts cytokine secretion of MSC-PBMC cocultures

Tidu et al., iScience *24*, 102683
June 25, 2021 
https://doi.org/10.1016/j.isci.2021.102683

iScience

CellPress
OPEN ACCESS

Article

# NFAT signaling in human mesenchymal stromal cells affects extracellular matrix remodeling and antifungal immune responses

Federico Tidu,[1,2] Marco De Zuani,[1] Shyam Sushama Jose,[1] Kamila Bendíčková,[1] Lukáš Kubala,[1,3] Frank Caruso,[4] Francesca Cavalieri,[4] Giancarlo Forte,[1] and Jan Frič[1,5,6,*]

## SUMMARY

**Mesenchymal stromal cells (MSCs) combined with calcineurin-nuclear factor of activated T cell (CN-NFAT) inhibitors are being tested as a treatment for graft-versus-host disease (GvHD). The immunosuppressive properties of MSCs seem beneficial; however, their response during fungal infection, which is an important cause of mortality in patients with GvHD , is unknown. We report that MSCs phagocytose the fungal component zymosan, resulting in phosphorylation of spleen tyrosine kinase (Syk), increase in cytosolic calcium levels, and ultimately, increase in NFAT1 nuclear translocation. RNA sequencing analysis of zymosan-treated MSCs showed that CN-NFAT inhibition affects extracellular matrix (ECM) genes but not cytokine expression that is under the control of the NF-κB pathway. When coculturing MSCs or decellularized MSC-ECM with human peripheral blood mononuclear cells (PBMCs), selective NFAT inhibition in MSCs decreased cytokine expression by PBMCs. These findings reveal a dual mechanism underlying the MSC response to zymosan: while NF-κB directly controls inflammatory cytokine expression, NFAT impacts immune-cell functions by regulating ECM remodeling.**

## INTRODUCTION

Mesenchymal stromal cells (MSCs) are multipotent cells that comprise the stromal fraction of many tissues and have key roles in supporting the hematopoietic stem cell niche (Méndez-Ferrer et al., 2010; Muguruma et al., 2006). Adipose tissue represents an important source of MSCs that can be harvested via noninvasive procedures and used for therapeutic applications (Mahmoudifar and Doran, 2015; Najar et al., 2010; Samsonraj et al., 2017). Indeed, the ability of MSCs to secrete immunosuppressive factors has attracted great attention for their potential therapeutic application for several immune disorders (Wang et al., 2019). For example, MSCs can be administered to patients undergoing hematopoietic stem cell transplantation to offer stromal support for the engrafted cells (Lazarus et al., 2005; Zhao and Liu, 2016). MSCs are also currently being tested as a supportive therapy to treat or prevent graft-versus-host disease (GvHD), owing to their ability to suppress innate and adaptive immune cell functions (Galipeau and Sensébé, 2018; Hashmi et al., 2016; Kim et al., 2018). Although the molecular mechanisms underlying these immunosuppressive properties are unclear, some data suggest that MSCs can promote regulatory T cell generation, inhibit NK cell cytotoxicity and proliferation, and inhibit dendritic cell (DC) maturation (Luz-Crawford et al., 2013; Spaggiari et al., 2008, 2009).

While the described functions of MSCs are crucial for GvHD therapy, they can potentially hamper the immune cell antifungal response resulting in a higher susceptibility to invasive fungal infection (von Bahr et al., 2012; Balan et al., 2014; Schmidt et al., 2017). *Aspergillus fumigatus* and *Candida albicans* are the leading cause of invasive fungal infection after transplantation (Koldehoff and Zakrzewski, 2005), and cells expressing the pattern recognition receptors (PRRs) target the β-glucans present in these fungi cell wall as the main pathogen-associated molecular pattern (PAMP) (Brown and Gordon, 2003).

The ability of MSCs to recognize and respond to various PAMPs or damage-associated molecular patterns (DAMPs) through self-expressed PRRs is well known (Hwa Cho et al., 2006; Najar et al., 2018; Waterman

[1]International Clinical Research Center, St. Anne's University Hospital, Pekařská 53, 656 91 Brno, Czech Republic

[2]Department of Biology, Faculty of Medicine, Masaryk University, Kamenice 5, 625 00 Brno, Czech Republic

[3]Institute of Biophysics of the Czech Academy of Sciences, Kralovopolska 135, 612 65 Brno, Czech Republic

[4]ARC Centre of Excellence in Convergent Bio-Nano Science and Technology, and the Department of Chemical Engineering, University of Melbourne, Parkville, VIC 3010, Australia

[5]Institute of Hematology and Blood Transfusion, U Nemocnice 2094/1, 128 20 Prague, Czech Republic

[6]Lead contact

*Correspondence: jan.fric@fnusa.cz

https://doi.org/10.1016/j.isci.2021.102683

et al., 2010; Yu et al., 2016). PRRs allow direct sensing of the tissue microenvironment for infection or tissue damage and their signaling cascade results in the secretion of cytokines that are important for orchestrating the immune response (Medzhitov et al., 1997; Tomchuck et al., 2008).

PRR-expressing cells recognize microbial constituents, thus forming a first line of defense against fungal infection. Zymosan particles have been widely used to model the innate immune response to fungal pathogens (Cao et al., 2019; Taylor et al., 2007a, 2007b). Although this preparation from yeast cell wall is composed of different molecules – including mannans, chitins, proteins, and lipids – β-glucans were reported to be its bioactive component (Di Carlo and Fiore, 1958). Zymosan recognition by the PRRs TLR2 and dectin-1 is followed by spleen tyrosine kinase (Syk) phosphorylation, phagocytosis, and consequent phagosome acidification (Gantner et al., 2003; Goodridge et al., 2011; Rogers et al., 2005). Syk kinase phosphorylation also causes calcium release from the endoplasmic compartment that subsequently induces conformational changes in the serine-threonine phosphatase calcineurin (CN). Such changes enable CN to bind and dephosphorylate nuclear factor of activated T cells (NFAT), which results in its nuclear translocation (Armstrong-James et al., 2018; Borriello et al., 2020; Goodridge et al., 2007; Herbst et al., 2015). Indeed, we and others have reported that zymosan elicits NFAT activation via PRR signaling in both DCs and macrophages (Fric et al., 2012; Goodridge et al., 2007).

Drugs developed to inhibit CN-NFAT activity, such as cyclosporine and tacrolimus (FK506), are routinely used in GvHD therapy because of their ability to suppress immune cell functions in transplanted tissues. While CN-NFAT inhibitors primarily target T cell activity, blocking this pathway also hampers the ability of myeloid cells to contain fungal infections, which are among the most severe complications to occur during GvHD therapy (Bendickova et al., 2017; Fric et al., 2012; Santus et al., 2017; Zelante et al., 2017).

Several clinical trials have tested the coadministration of NFAT inhibitors (cyclosporine or tacrolimus) and MSCs as a GvHD therapy to maximize immune suppression and improve prognosis (Balan et al., 2014; Fisher et al., 2019). However, the molecular events occurring in MSCs exposed to fungal PAMPs and the consequences on immune cell functions remain largely unknown. This gap in knowledge must be filled, as NFAT might be activated on PRR stimulation in MSCs and play a role in immunomodulatory processes. In the present study, we aimed to shed light on the molecular mechanisms orchestrating the MSC response to fungal PAMPs and the effects on immune cell function. To do so, we investigated the response of human adipose-derived MSCs (Ad-MSCs) to zymosan stimulation and the consequences on CN-NFAT signaling.

## RESULTS

### Phagocytosis of zymosan by Ad-MSCs leads to cytokines expression

Several studies have shown that Ad-MSCs express functional PRRs. However, their ability to recognize and respond against fungal constituents has been poorly described. To verify whether cultured Ad-MSCs can mount an antifungal response, we stimulated the cells using zymosan. We then assessed cytokine expression at different time points after stimulation. We observed a significant increase in mRNA expression of the interleukins (IL) *IL-1B*, *IL2*, *IL-6*, *IL-8*, and *IL12p40* and the antimicrobial enzyme indoleamine 2, 3-dioxygenase 1 (*IDO*), 4 h after zymosan stimulation when compared with untreated cells (Figure 1A). Moreover, we measured the mRNA expression of *IL6* and *IL8*, after TLR1/6 and TLR2/6 ligation in MSCs, in the monocytic cell line THP-1 and in THP-1-derived macrophages (Figure S1).

As a particulate ligand, zymosan usually engages phagocytic processes in myeloid cells (Herre et al., 2004; Rogers et al., 2005). To understand how MSCs recognize zymosan, we stimulated Ad-MSCs again, this time using zymosan conjugated to a pH-sensitive dye (phrodo-Zymosan). By this approach, we observed internalization followed by phagosome acidification occurring just 2 h after stimulation (Figures 1B and 1C). Furthermore, phagocytosis was inhibited in cells preincubated with cytochalasin D, a drug used to inhibit cytoskeletal rearrangements and phagocytic processes (Figure 1C). We also confirmed the endocytic ability of MSCs when using dextran with different molecular weights. By confocal imaging (Figure 1D) and fluorescence-activated cell-sorting (FACS) analysis (Figure 1E), we found that MSCs could internalize dextran chains in the molecular weight range 3–40 kDa; incubating the cells at 4°C significantly inhibited endocytosis, confirming the active phagocytic process.

In summary, we found that MSCs can recognize and phagocytose zymosan particles. The phagocytic events observed after 2 h of stimulation with zymosan were followed by increased mRNA expression of *IL-8*, *IL-6*,

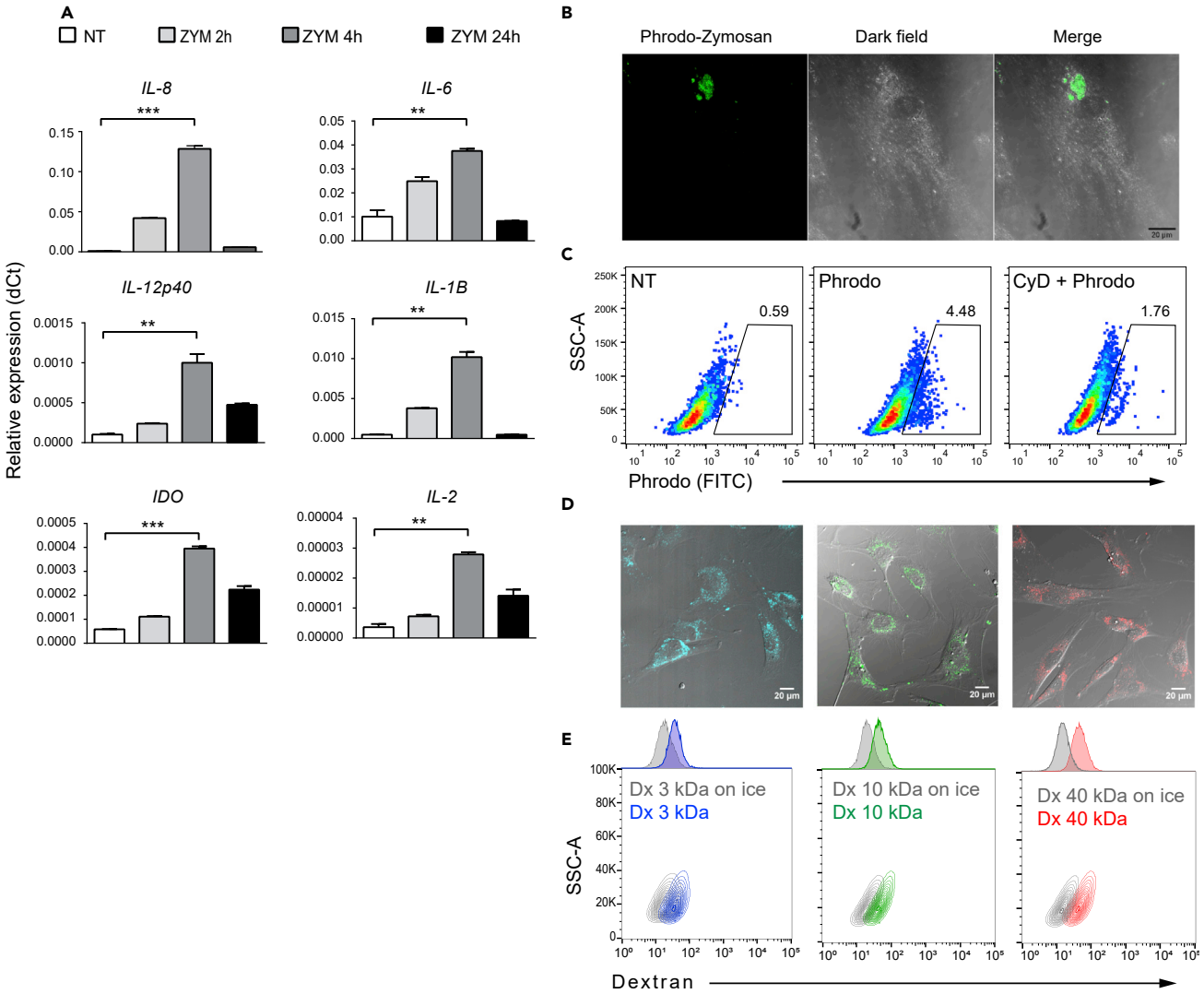


**Figure 1. Phagocytosis of zymosan by Ad-MSCs leads to cytokines expression**

(A) *IL-8*, *IL-6*, *IL12p40*, *IL-1B*, *IDO* and *IL-2* mRNA expression in Ad-MSCs stimulated with 10 μg/mL zymosan (ZYM) at different time points. The data represent the relative expression compared to the housekeeping gene (GAPDH). The data are representative of two independent experiments.

(B) Confocal images showing pHrodo-labeled zymosan internalization by hTERT-MSCs. Fluorescence emission indicates phagosome acidification.

(C) Flow cytometry analysis showing hTERT-MSCs ability to phagocytose pHrodo-zymosan compared with untreated cells (middle and left panels, respectively). Right panel shows decreased phagocytic ability for cells pretreated with cytochalasin D.

(D) Confocal images showing hTERT-MSC-mediated endocytosis of dextran chains in the tested range 3–40 kDa.

(E) Flow cytometry analysis showing the ability of hTERT-MSCs to internalize dextran chains at the indicated molecular weight (kDa). Gray shading represents the negative control, where endocytic processes were inhibited at 4°C. $^{**}p < 0.01$, $^{***}p < 0.005$; two-tailed unpaired t test.

*IL-12p40*, *IL-1B*, *IDO*, and *IL-2*, suggesting that MSCs are capable of mounting an inflammatory response when exposed to fungal constituents.

## A PRR-driven response to zymosan results in calcineurin-NFAT activation

Having shown that Ad-MSCs can respond to zymosan, we next wanted to understand the nature of the underlying signaling pathway. To do so, we analyzed the expression of dectin-1, a well-characterized zymosan receptor and PRR (Gantner et al., 2003; Goodridge et al., 2007), in Ad-MSCs. Confocal microscopy analysis indeed revealed that dectin-1 is expressed by Ad-MSCs (Figure 2A). HEK-293 cells were used as a dectin-1 negative control, while the positive control was obtained by transfecting HEK-293 cells with a plasmid carrying the dectin-1-coding sequence (Figure S2). Moreover and as already shown for DCs, western blot

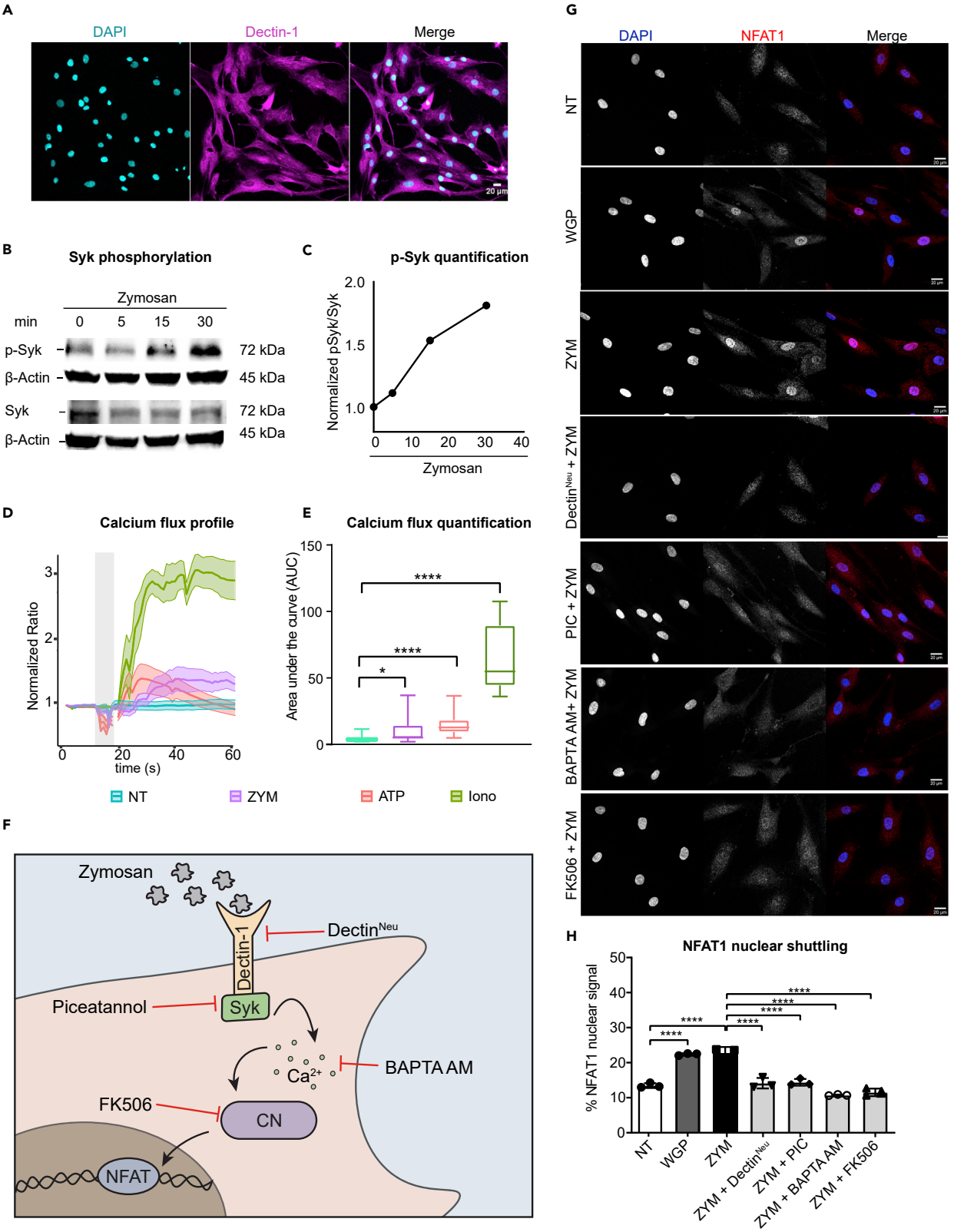
A
DAPI
Dectin-1
Merge
20 µm
B
Syk phosphorylation
Zymosan
min
0
5
15
30
p-Syk
72 kDa
β-Actin
45 kDa
Syk
72 kDa
β-Actin
45 kDa
C
p-Syk quantification
Normalized pSyk/Syk
2.0
1.5
1.0
0
10
20
30
40
Zymosan
D
Calcium flux profile
Normalized Ratio
3
2
1
0
20
40
60
time (s)
NT
ZYM
E
Calcium flux quantification
Area under the curve (AUC)
150
100
50
0
****
****
*
ATP
Iono
F
Zymosan
Dectin-1
Dectin^Neu
Piceatannol
Syk
Ca2+
BAPTA AM
FK506
CN
NFAT
G
DAPI
NFAT1
Merge
NT
WGP
ZYM
Dectin^Neu + ZYM
PIC + ZYM
BAPTA AM+ ZYM
FK506 + ZYM
H
NFAT1 nuclear shuttling
% NFAT1 nuclear signal
50
40
30
20
10
0
****
****
****
****
****
****
NT
WGP
ZYM
ZYM + Dectin^Neu
ZYM + PIC
ZYM + BAPTA AM
ZYM + FK506

**Figure 2. Ad-MSCs engage a PRR-driven response to zymosan leading to CN-NFAT activation**

(A) Immunofluorescent dectin-1 labeling in hTERT-MSCs.

(B) Western blot analysis of zymosan-induced Syk phosphorylation (p-Syk) and total Syk expression (Syk) in hTERT-MSCs. β-Actin was used as a loading control.

(C) Western blot quantification showing the band intensity ratio for pSYK/Syk.

(D) Live calcium imaging in Ad-MSCs stimulated with zymosan (ZYM), ionomycin (Iono), ATP, or no treatment (NT). A calcium tracker was used. The calcium dynamics are presented as fluorescence intensity plotted against time, where the values of fluorescence are normalized to the fluorescence signal at t = 0 s.

(E) Calcium flux quantification. The graph represents the area under the curve (AUC) for the untreated (NT), zymosan (ZYM), ionomycin (Iono) and ATP groups. The data are representative of three independent experiments. The data were analyzed against NT by Kruskal-Wallis test followed by Dunn's multiple comparison test.

(F) Schematic of dectin1-NFAT signaling cascade with inhibitors.

(G) Representative confocal images of NFAT1 subcellular localization in Ad-MSCs untreated, WGP-stimulated, or stimulated with zymosan in presence and absence of FK506, dectin-1 neutralizing antibody ($Dectin^{Neu}$), Piceatannol (PIC) or BAPTA AM.

(H) Quantification of NFAT1 nuclear/cytoplasmic ratio (expressed as percentage). A total of 30 images from three independent experiments were analyzed and compared by one-way ANOVA followed by Sidak's multiple comparison test. ****$p < 0.0001$.

analysis revealed that zymosan binding Ad-MSCs resulted in the phosphorylation of Syk kinase — a known consequence of dectin-1 stimulation (Figures 2B and 2C). Furthermore, live imaging of MSCs stained with a calcium-sensor dye revealed that zymosan stimulation induced a significant increase in cytosolic calcium levels compared with unstimulated cells. Adenosine triphosphate (ATP) and a calcium ionophore (ionomycin) were used as the positive controls (Figures 2D and 2E). These data thus support that Ad-MSCs adopt a PRR-driven response to zymosan that might result in NFAT activation. In fact, we and others have reported that the CN-NFAT pathway is engaged during the PRR-dependent antifungal response (Bendíčková et al., 2020; Goodridge et al., 2007) (Figure 2F). To verify whether Ad-MSCs engage the CN-NFAT axis in response to zymosan, we again stimulated the cells using the particulate ligand and monitored NFAT subcellular localization by confocal microscopy. We observed that zymosan induces a significant increase in NFAT1 nuclear localization compared with the untreated control (Figures 2G and 2H). This observation was confirmed using the whole glucan particles (WGP), a PAMP binding specifically to dectin-1. Moreover, when cells were pretreated with the CN-NFAT inhibitor, we observed a significant decrease in zymosan-induced NFAT nuclear shuttling. Consistently with our hypothesis, similar inhibitory effects were also obtained by using a dectin-1-neutralizing antibody, the Syk inhibitor piceatannol or the calcium chelator BAPTA acetoxymethyl ester (BAPTA AM) (Figures 2G and 2H). NFAT shuttling was also dependent on calcium dynamics, as observed by structured illumination microscopy and confocal analyses (Figures S3A–S3C).

Altogether, these findings suggest that Ad-MSCs can activate a PRR-dependent response to zymosan. This response relies on dectin-1 receptor, Syk kinase activation, a subsequent increase in cytosolic $Ca^{2+}$ levels and NFAT1 nuclear translocation.

## Zymosan elicits a PRR-driven response in Ad-MSCs that culminates in NFAT and NF-κB activation

To identify the gene signature associated with zymosan stimulation and the relevance of CN-NFAT pathway in activated MSCs, we performed bulk RNA sequencing on primary human Ad-MSCs isolated from three human donors. First, we confirmed the MSC phenotype by analyzing the expression of mesenchymal markers by flow cytometry (Figure S4). Here, we found that Ad-MSCs from all three donors expressed similar CD105, CD90, and CD73 levels and lacked hematopoietic marker CD45, CD14, and HLA-DR expression. Comparable levels of expression were also observed in immortalized adipose-derived MSCs (hTERT-MSCs).

Next, we analyzed global gene expression in primary Ad-MSCs left untreated or stimulated for 6 h with zymosan. To determine which genes are involved in the MSC "antifungal" response, we analyzed the differentially expressed genes (DEGs) in zymosan-treated versus untreated samples (Figures 3A and 3B). Gene ontology analyses on the biological processes of the 265 upregulated genes revealed that zymosan induced the activation of genes annotated as "inflammatory response" and "response to bacterium" (Figures 3C and S5). In particular, the expression of the pro-inflammatory cytokines *IL1B*, *IL6* and *IL8* was increased by approximately 5-, 3- and 8-fold, respectively. In keeping with our hypothesis, gene set enrichment analysis (GSEA) revealed a correlation between zymosan treatment and the upregulation of genes belonging to the NFAT and NF-κB families (Figure 3D). We also identified that several gene sets involved in the PRR response were enriched in the zymosan-treated group, including the "MYD88 cascade,"

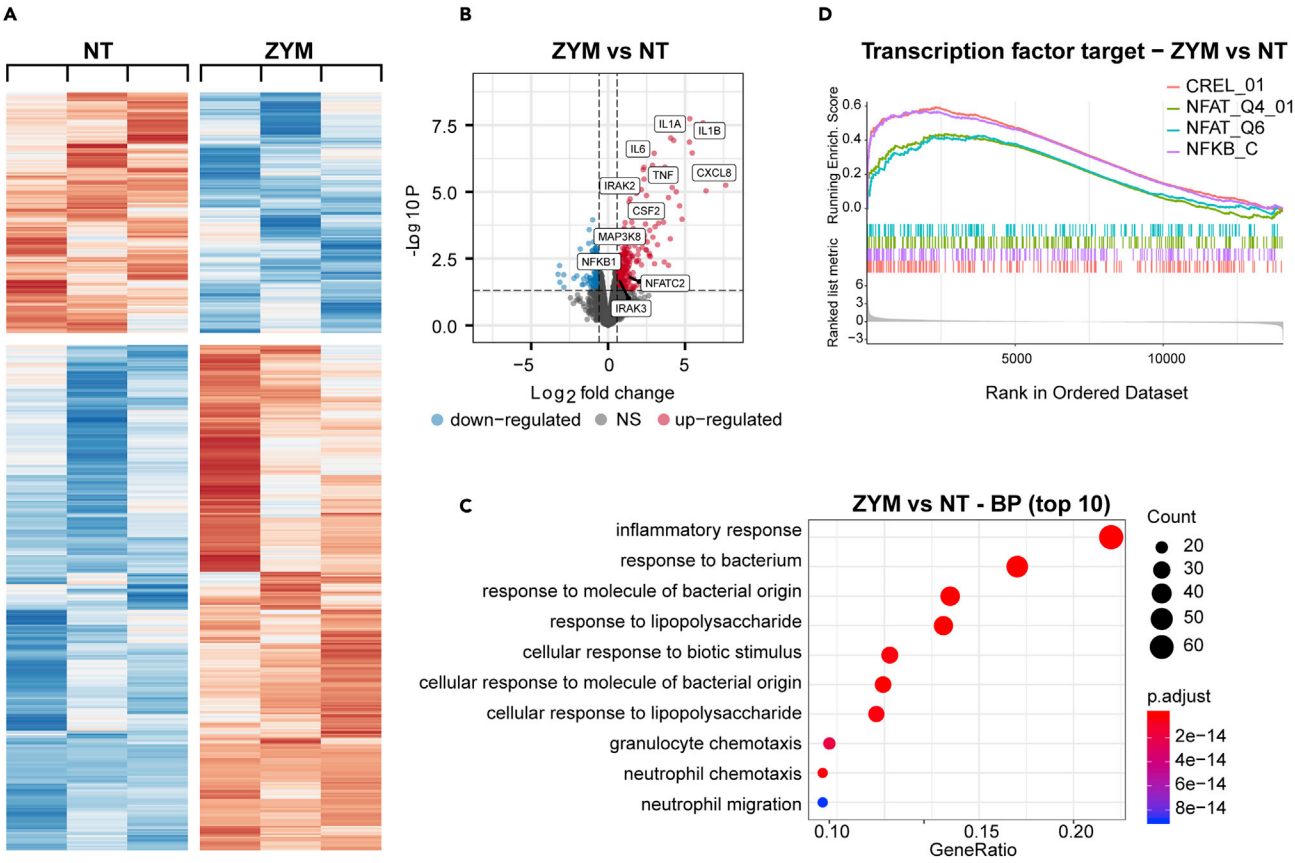


**Figure 3. Zymosan elicits a PRR-driven response in Ad-MSCs that culminates in NF-κB activation**

(A–D) RNA-sequencing analysis of zymosan-treated (ZYM) and untreated (NT) Ad-MSCs (fold change ≥ |1.5| and a p value ≤ 0.05). (A) A heatmap representing differentially expressed genes (DEGs) between NT and ZYM. Colors indicate the row-scaled log2FC. (B) A volcano plot representing all the genes as a function of log2 fold changes (x axis, log2FC) and p value (y axis, log P). Genes highlighted in red are DEGs with log2FC > 0.58 and a p value < 0.05. Genes highlighted in blue are DEGs with log2FC < −0.58 and a p value < 0.05. (C) Gene ontology analysis on biological processes (BP) of significantly upregulated genes. (D) Gene set enrichment analysis (GSEA) performed on an unfiltered gene list.

"CLEC7A-dectin1 signaling," the "TLR4 cascade," and the "TLR1:TLR2 cascade" (Figure S6). Altogether, these data confirm that zymosan elicits an inflammatory response in Ad-MSCs that is mediated by TLR and dectin-1 signaling and that culminates in NFAT and NF-κB activation.

## NFAT regulates the expression of genes involved in extracellular matrix (ECM) metabolism

The CN-NFAT axis has a prominent role in the myeloid cell response to fungal infection (Fric et al., 2012). As our data thus far suggest that NFAT is activated in Ad-MSCs in response to zymosan and the signaling cascade is similar to that observed in myeloid cells, we investigated the effects of NFAT inhibition on the MSC antifungal response. For this purpose, we compared the DEGs between zymosan-stimulated cells cultured in the presence or absence of the NFAT inhibitor, FK506. Heatmap and volcano plot representations (Figures 4A and 4B) highlighted clusters of DEGs. Comparing the DEGs between the two treatment groups, we found that NFAT inhibition impacted the expression of some genes involved in ECM metabolism, including cell-migration-inducing hyaluronidase 1 (*CEMIP*), hyaluronan synthase 1 (*HAS1*) and hyaluronan synthase 3 (*HAS3*). These results were confirmed by real-time quantitative polymerase chain reaction for the genes *HAS1* and *CEMIP* (Figure S7).

Contrary to our initial hypothesis, inhibiting CN-NFAT did not affect genes involved in cytokine production. Meanwhile, GSEA analysis confirmed that gene sets associated with ECM deposition were impacted by FK506 treatment (Figure 4C).

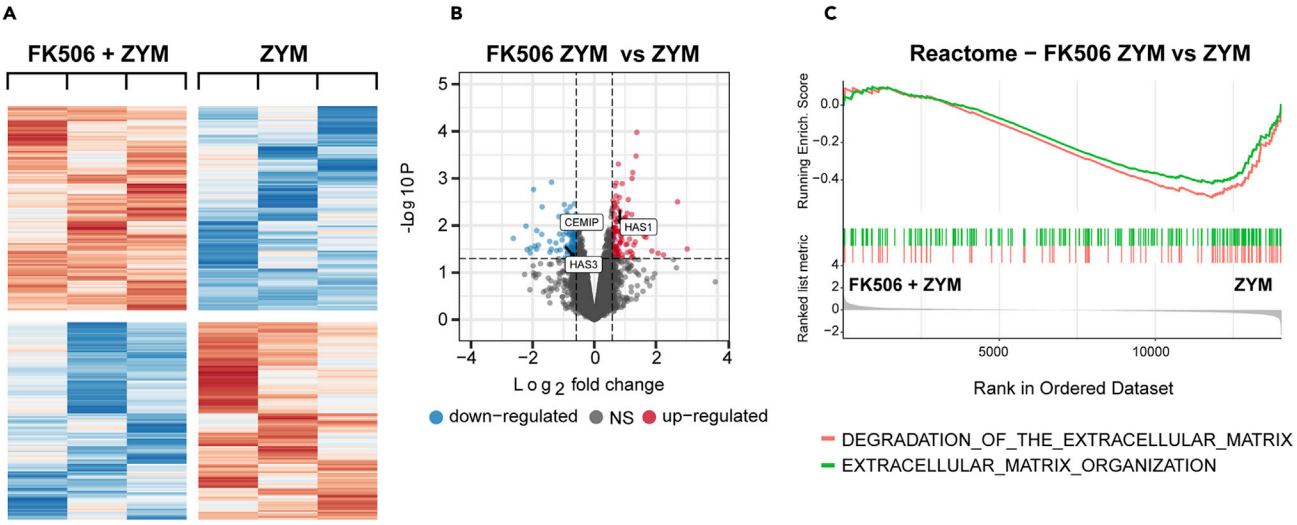


**Figure 4. NFAT regulates the expression of genes involved in hyaluronan metabolism**

(A–C) RNA-sequencing analysis of FK506 + ZYM vs ZYM. (A) Heatmap representing DEGs between FK506 + ZYM and ZYM samples. Colors indicate the row-scaled log2FC (B) Volcano plot representing all the genes as a function of log2 fold changes (x axis, log2FC) and p value (y axis, log P). Red and blue labeling is as for Figure 3B. (C) GSEA performed on an unfiltered gene list.

Altogether, our RNA sequencing data suggest that Ad-MSCs can respond to fungal PAMPs through PRR activation and the expression of several inflammatory cytokines. NFAT activation observed in response to zymosan is not directly associated with cytokine expression; instead, this is likely controlled by NF-κB. Nevertheless, NFAT seems to have a specific role in the expression of genes involved in the metabolism of the ECM, especially hyaluronan.

## Zymosan induces NF-κB activation and subsequent IL-6 and IL-8 expression in MSCs

Thus far, our RNA sequencing data suggest that transcription factors other than NFAT are responsible for zymosan-induced cytokine expression. Because of the correlation observed between zymosan stimulation and the upregulation of genes associated with NF-κB signaling, we decided to focus on the role of this transcription factor in Ad-MSCs. We first monitored the expression of key proteins associated with NF-κB activation and dectin-1 signaling cascade (Figure 5A).

Next, we monitored the nuclear translocation of NF-κB p65 subunit by performing an ELISA on nuclear extracts of Ad-MSCs stimulated with zymosan or left untreated. The experiments revealed that zymosan significantly induced NF-κB p65 subunit nuclear translocation compared with untreated samples (Figure 5B). Furthermore, we confirmed NF-κB transcriptional activity in MSCs upon zymosan stimulation, using a reporter line based on luciferase expression under the control of the NF-κB promoter. When we stimulated the hTERT-MSC reporter line with zymosan, we observed significantly increased luciferase activity compared to the untreated group. In addition, zymosan-induced luciferase activity was lower in cells pretreated with the NF-κB inhibitor TPCA-1 (Figure 5C).

To correlate our RNA sequencing data with protein secretion, we performed enzyme-linked immunosorbent assays (ELISAs) for IL-6 and IL-8 cytokines, which were two of the most up-regulated cytokines (3- and 8-fold up-regulation compared with untreated samples, respectively) in the zymosan-treated group. Using supernatants of MSCs untreated or treated with zymosan, we confirmed that zymosan indeed induced IL-6 and IL-8 secretion. Moreover, IL-6 and IL-8 expression was markedly reduced upon zymosan stimulation when the cells were exposed to the NF-κB inhibitor TPCA-1 but not when exposed to the NFAT inhibitor FK506 (Figures 5D and 5E).

In summary, these results confirm that Ad-MSCs express several key proteins involved in NF-κB signaling through the dectin-1 receptor. In this context, zymosan induces NF-κB signaling, which culminates with NF-κB p65 subunit nuclear import, and IL-6 and IL-8 expression. Together with our RNA sequencing data, these results point to a dual mechanism underlying the Ad-MSC response to fungal PAMPs. On the one side,

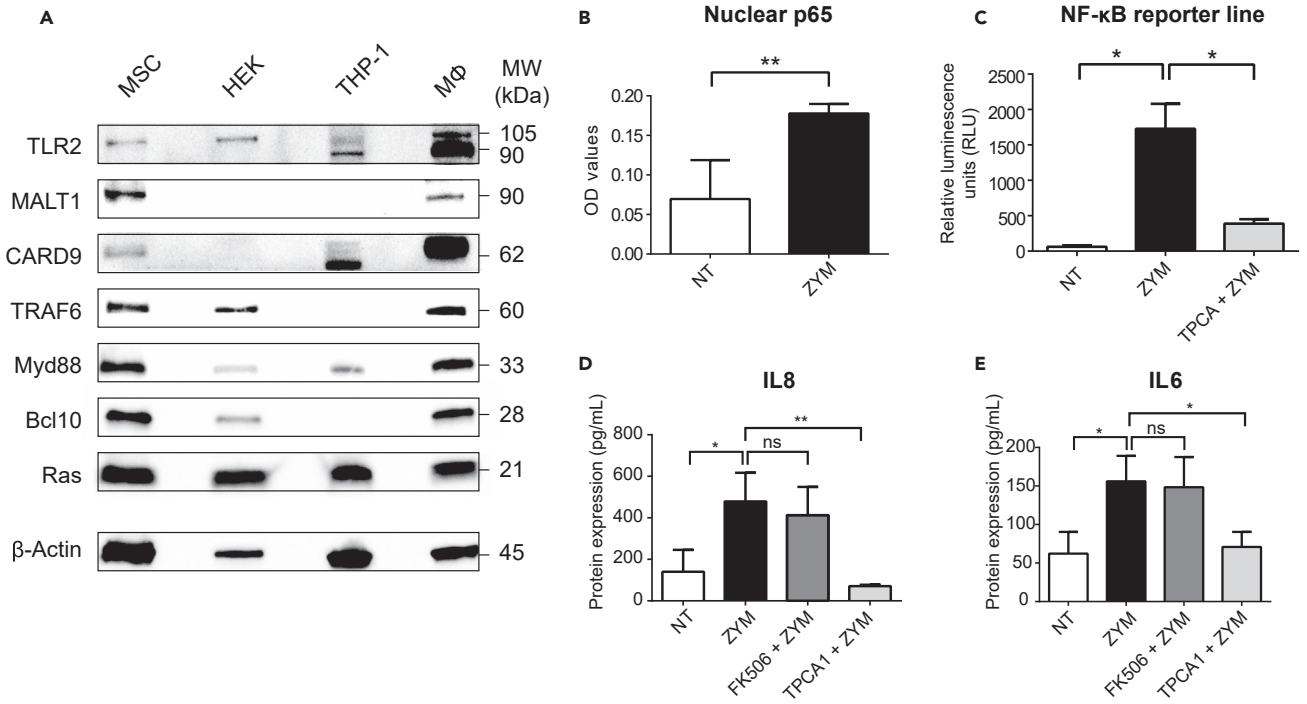


**Figure 5. Zymosan induces the activation of NF-κB, which controls IL-6 and IL-8 protein expression**

(A) Western blot analyses of TLR2, MALT1, CARD9, TRAF6, Myd88, Bcl10, and Ras in hTERT-MSCs, HEK-293, THP-1, and THP-1-derived macrophages. β-Actin was used as loading control.

(B) NF-κB p65 subunit expression in nuclear extracts of hTERT-MSCs untreated (NT) or stimulated for 10 min with 10 μg/mL zymosan (ZYM). The data are representative of four independent experiments and were analyzed by two-tailed unpaired t-tests.

(C) The relative luminescence units (RLU) of MSC NF-κB reporter cells stimulated for 18 h with zymosan in the presence or absence of TPCA-1 inhibitor. The data are representative of three independent experiments and were analyzed by two-tailed unpaired t test. *$p < 0.05$, **$p < 0.01$.

(D) IL8 protein expression in supernatants of Ad-MSCs untreated or stimulated with zymosan, zymosan + FK506 or zymosan + TPCA-1 for 18h. The data represent the means of three independent experiments and were analyzed by one-way ANOVA followed by Sidak's multiple comparison test.

(E) IL6 protein expression in supernatants of Ad-MSCs untreated or stimulated with zymosan, zymosan + FK506 or zymosan + TPCA-1 for 18h. The data represent the means of three independent experiments and were analyzed by one-way ANOVA followed by Sidak's multiple comparison test. *$p < 0.05$, **$p < 0.01$.

these cells produce inflammatory cytokines, mainly under the control of the NF-κB pathway. On the other side, zymosan-stimulated and calcium-driven NFAT signaling regulates the expression of genes involved in ECM remodeling.

## Selective NFAT inhibition in Ad-MSCs impacts the peripheral blood mononuclear cell antifungal response

Our data thus far support that CN-NFAT inhibition affects the expression of genes involved in ECM remodeling. Considering that aberrant expression of ECM molecules or their fragments can impact on immune cell activation (Sorokin, 2010), our final analyses aimed to determine whether NFAT-driven changes on ECM composition affect immune cells during zymosan stimulation. For this purpose, we established an hTERT-MSC cell line expressing the NFAT inhibitory peptide VIVIT fused to GFP. We inserted the original VIVIT-GFP sequence developed by *Aramburu* (Aramburu, 1999) into a lentiviral backbone. In our system, conditional VIVIT-GFP expression was regulated via a Tet3G-doxycycline (DOX) system (Figures 6A and 6B).

We first validated the responsiveness of the MSC-VIVIT line by assessing GFP expression on DOX stimulation. Flow cytometry analysis showed that even at the lowest concentration tested (0.125 μg/mL), DOX induced VIVIT-GFP expression in nearly all cells (Figure 6C). To confirm that VIVIT-GFP expression was sufficient to limit NFAT nuclear translocation, we treated MSC-VIVIT with either DOX for 18 h ($MSC^{VIVIT+}$) or left the cells untreated ($MSC^{VIVIT-}$). We then stimulated both samples with zymosan to induce NFAT nuclear translocation. Confocal analysis confirmed that pretreatment with DOX to stimulate VIVIT-GFP significantly inhibited NFAT1 nuclear

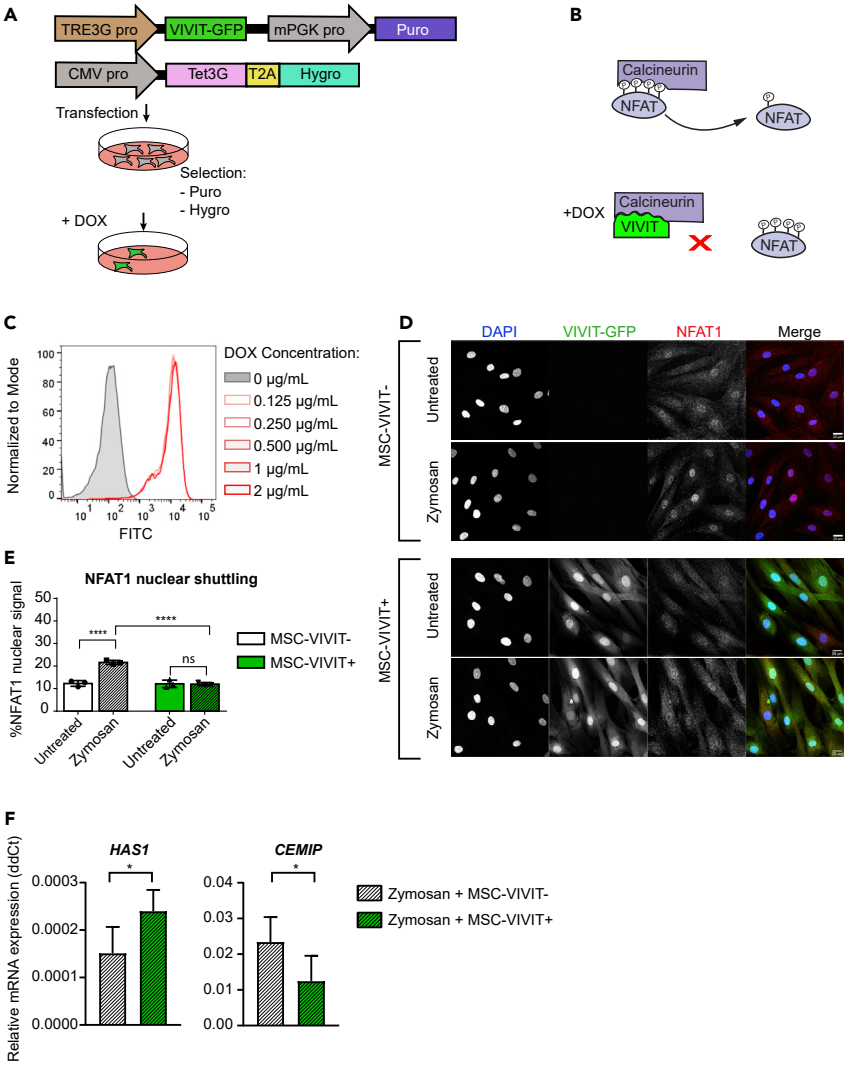


**Figure 6. VIVIT-MSCs line characterization**

(A) Schematic of the VIVIT-TET expression vectors and the strategy used to obtain the stable line.

(B) Mechanism of action of VIVIT peptide.

(C) FACS analysis of VIVIT expression in MSC after 0.125–2 µg/mL doxycyline (DOX) treatment.

(D) VIVIT-mediated inhibition of NFAT nuclear translocation was visualized by confocal microscopy. The top panel shows untreated cells or cells stimulated with zymosan in the absence of DOX (MSC-VIVIT-). The bottom panel shows the same conditions after DOX stimulation (MSC-VIVIT+).

(E) Quantification of the NFAT1 nuclear signal. A total of 30 images from three independent experiments were used for the analysis. The data were analyzed by one-way ANOVA followed by Sidak's multiple comparison test. ****$p < 0.0001$.

(F) *HAS1 and CEMIP* mRNA expression in MSC-VIVIT + or MSC-VIVIT-stimulated with 10 µg/mL zymosan. The data represent the relative expression compared with the housekeeping gene (*ACTB*). The data are representative of three independent experiments. The data were analyzed by Mann-Whitney test. *$p < 0.5$.

translocation induced by zymosan compared to samples that were not pretreated with DOX (Figures 6D and 6E). To validate our model, we analyzed mRNA levels of the NFAT-dependent genes *HAS1* and *CEMIP* and of the NF-kB-dependent cytokines IL-6 and IL-8 (Figures 6F and S8) in both zymosan-treated $MSC^{VIVIT+}$ and $MSC^{VIVIT-}$. In accordance with our hypothesis, NFAT inhibition via VIVIT peptide affected the expression of *HAS1* and *CEMIP*, while no significant differences were observed for the NF-κB-regulated genes *IL6* and *IL8*.

Once validated, we tested whether inhibition of NFAT in the $MSC^{VIVIT}$ line affected MSC cross talk with immune cells when exposed to zymosan. To address this, we analyzed cytokine secretion via cytometric bead

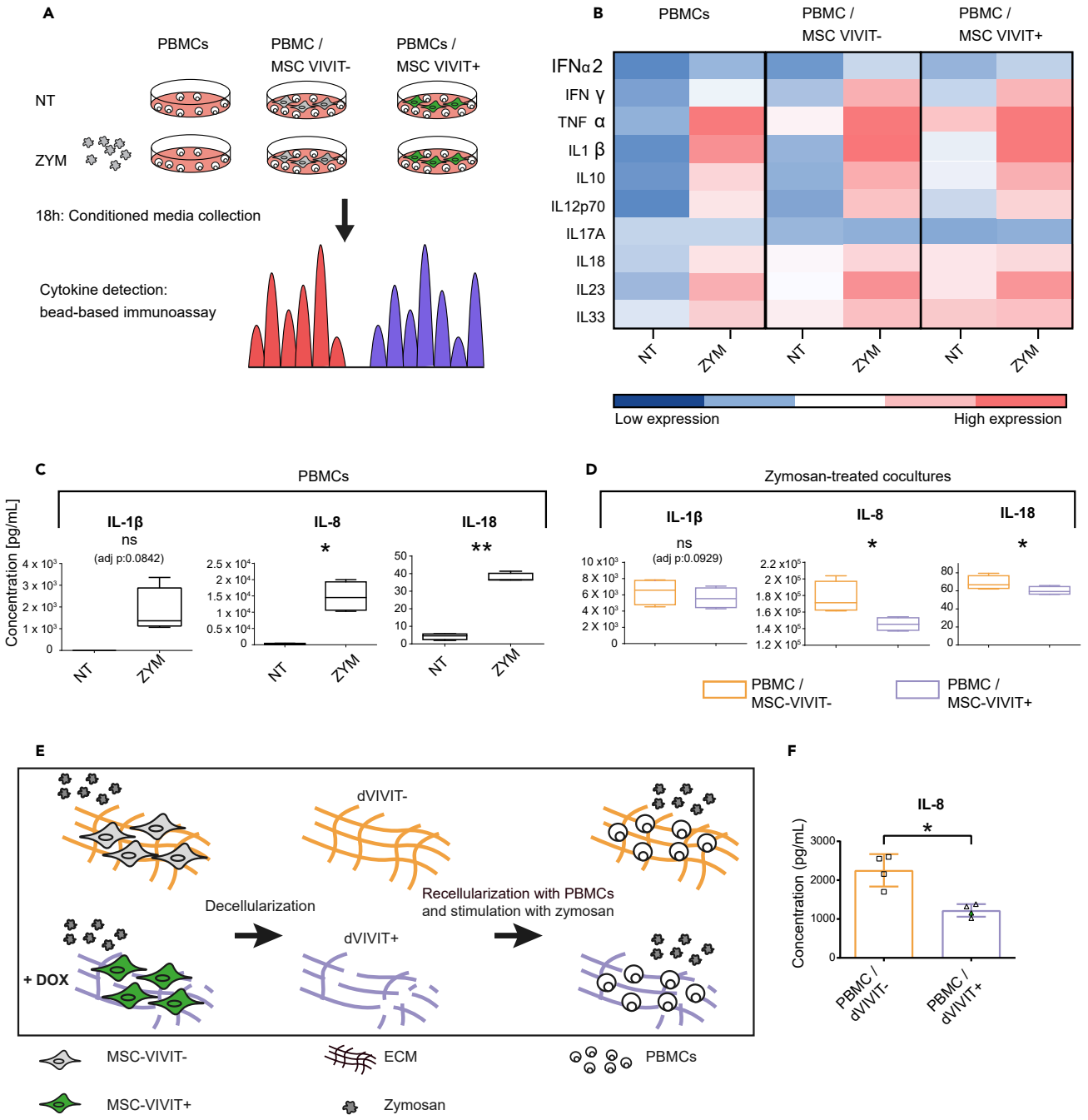


**Figure 7. Selective inhibition of NFAT in MSCs impacts PBMCs antifungal response**

(A) Schematic of the peripheral blood mononuclear cell (PBMC) coculture experimental design.

(B) A heatmap representing the cytokine expression triggered by zymosan in PBMCs, cocultured PBMCs and VIVIT-MSCs without doxycycline (PBMC/MSC-VIVIT-) and cocultured PBMCs and MSC with doxycycline (PBMC/MSC VIVIT+).

(C) Graphs comparing cytokine expression detected in conditioned media (CM) of untreated PBMCs (NT) and PBMCs treated with zymosan (ZYM). The data were analyzed by repeated-measures (RM) one-way ANOVA with the Greenhouse-Geisser correction followed by the Sidak's multiple comparison test. *adj. $p < 0.05$, ** adj. $p < 0.01$.

(D) Cytokine expression in "PBMC/MSC-VIVIT-" and "PBMC/MSC-VIVIT+" CM. The data were analyzed by RM one-way ANOVA with the Greenhouse-Geisser correction followed by the Sidak's multiple comparison test. *adj. $p < 0.05$.

(E) Schematic of the decellularization experimental design.

(F) IL8 protein levels in supernatants of zymosan-treated (10μg/mL) PBMC/dVIVIT+ and PBMC/dVIVIT-. PBMCs isolated from 4 different donors were used for the analysis. The data were analyzed by Paired t test. *$p < 0.05$.

immunoassay in the supernatants of three different groups: (1) peripheral blood mononuclear cells (PBMCs) alone, (2) cocultures of PBMCs together with $MSC^{VIVIT+}$, and (3) coculture of PBMCs together with $MSC^{VIVIT-}$. The three groups were either stimulated with zymosan or left untreated (Figure 7A). We observed that zymosan triggered the production of several inflammatory cytokines in all three groups (Figure 7B).

Further analyses revealed that the zymosan-treated PBMCs released a significantly higher amount of IL-8, IL-18, IL-6, IL-33, and IL-17A compared with the untreated control cells (Figures 7C and S9). This increase in expression of proinflammatory cytokines is in keeping with an antifungal response mounted by PBMCs.

We next investigated whether inhibiting CN-NFAT affect cytokine expression in MSCs in coculture with human PBMCs. Here, we compared the cytokine expression in zymosan-treated cocultures of PBMC with $MSC^{VIVIT+}$ or $MSC^{VIVIT-}$ (Figures 7D and S10). Strikingly, we found that conditioned media from PBMC/$MSC^{VIVIT+}$ presented lower levels of IL-8 (adj. p value = 0.03), IL-18 (adj. p value = 0.04), and, to some extent, IL-1β (adj. p value = 0.09). This set of experiments showed that selective NFAT inhibition in MSCs significantly affects the expression of IL-8 and IL-18, two important cytokines produced also in response to fungal infection. The observed differences are likely dependent on altered ECM composition.

As we demonstrated, NFAT inhibition via VIVIT peptide resulted in altered expression of genes involved in ECM remodeling. To evaluate the effect of ECM remodeling on immune cell response to zymosan, we harnessed the decellularized matrices (dECMs) secreted by MSCs. Therefore, we stimulated $MSC^{VIVIT+}$ or $MSC^{VIVIT-}$ with zymosan for seven days; we then removed the cellular component as per the protocol published by Ji et al. (Ji et al., 2018) and obtained dECM produced by either $MSC^{VIVIT+}$ (dVIVIT+) or $MSC^{VIVIT-}$ (dVIVIT-) (Figure S11). Finally, we seeded freshly isolated PBMCs onto dVIVIT+ or dVIVIT- and stimulated the cells with zymosan for 18 h (Figure 7E). Cytokine analysis performed on cell supernatants revealed that PBMCs seeded on dVIVIT+ released significantly lower amount of IL-8 compared with the PBMCs seeded onto dVIVIT- (Figure 7F).

Altogether, these results corroborate with our observations in coculture, where PBMC/$MSC^{VIVIT+}$ secreted lower amount of IL-8 compared with PBMC/$MSC^{VIVIT-}$.

## DISCUSSION

MSCs have been the subject of numerous trials owing to their ability to modulate the inflammatory microenvironment. In recent years, great efforts have been made to investigate MSC properties in the context of GvHD, where the coadministration of MSCs and CN inhibitors aims at maximizing the immunosuppression, thus improving patients' clinical course. Nonetheless, the immunosuppressive regimen is also associated with higher risk of fungal infections, including severe life-threatening complications for patients with GvHD (Galipeau and Sensébé, 2018; Imbert et al., 2016). Here, we investigated the molecular events underlying the MSC response to fungal infection. To do so, we monitored MSC gene expression profiles after exposure to the fungal component zymosan, and the effect on the crosstalk with immune cells. We found that Ad-MSCs phagocytose zymosan, which causes the phosphorylation of the tyrosine kinase Syk and increase in cytosolic calcium concentration. This cascade of events results in NFAT nuclear translocation and the expression of genes involved in ECM metabolism. Contextually, zymosan also elicits NF-κB activation, which induces cytokines expression.

Zymosan is associated with phagocytosis and inflammatory cytokine production in myeloid cells (Gantner et al., 2003). Here, we have observed that Ad-MSCs rapidly internalized zymosan particles, which resulted in the expression of several proinflammatory cytokines, including IL-6 and IL-8. MSC phagocytic ability was previously described in another study (Schmidt et al., 2017), where the authors described MSCs' phagocytosis of *A. fumigatus* conidia. However, in that case, MSCs were unable to release significant amounts of inflammatory cytokines upon fungal recognition. This discrepancy with our results might be owing to the early time point chosen by the study authors (6 h) for their protein analyses.

In keeping with observations performed in myeloid cells (Goodridge et al., 2009; Kerrigan and Brown, 2010), here, we show that also stimulating Ad-MSCs with zymosan results in Syk kinase phosphorylation, an increase in cytosolic $Ca^{2+}$ concentration and then NFAT1 nuclear translocation. The same events have been described in murine DCs and neutrophils as well as in human macrophages and monocytes,

where the CN-NFAT pathway is engaged upon fungal infection and elicits the expression of antifungal cytokines and cytokine-induced proteins, such as TNF-α, pentraxin 3, IL-2, IL-10, and IL-12p70. Although both MSCs and myeloid cells can phagocytose fungal components and activate the CN-NFAT pathway, the outcomes are starkly different. In fact, inhibiting CN-NFAT in Ad-MSCs had no impact on zymosan-induced cytokine expression, as demonstrated by RNA sequencing and ELISA on secreted IL-6 and IL-8. To complement these data, we also observed by cytokine profile and luciferase reporter a predominant role of NF-κB in inducing IL-6 and IL-8 production. These results suggest that although the signaling cascade leading to NFAT activation is similar in myeloid cells and Ad-MSCs, the genetic programs elicited by its activation might largely differ.

RNA sequencing analysis subsequently elucidated a specific role for CN-NFAT in regulating a cluster of genes involved in ECM metabolism in Ad-MSCs, including the hyaluronan-associated genes *HAS1*, *HAS3*, and *CEMIP*.

Ultimately, our findings reveal that the MSC response to zymosan is characterized by two distinct, but intertwined events. On the one hand, zymosan elicits the expression of proinflammatory cytokines, mostly dependent on NF-κB pathway. On the other hand, simultaneous CN-NFAT activation dictates changes in hyaluronan-associated genes, which likely impacts on ECM composition.

This observation can explain one of the mechanisms exploit by MSCs for their immunosuppressive properties. Indeed, aberrant expression of ECM components can influence immune cell functions (Sorokin, 2010). In particular, hyaluronan is abundant in inflamed tissues (Edelstam et al., 1992), where it interacts with several other ECM molecules that are present at injury sites (Day and Prestwich, 2002; Jiang et al., 2007). Among the genes regulated by NFAT in MSCs, *HAS1* is responsible for *de novo* hyaluronan synthesis, while *CEMIP* is a hyaluronidase involved in hyaluronan depolymerization and the formation of hyaluronic acid (HA) fragments (Nagaoka et al., 2015). Such fragments can be recognized by TLRs and thus perpetuate inflammatory signals (Scheibner et al., 2006; Taylor et al., 2007a, 2007b; Tesar et al., 2006). Moreover, it has been shown that HA can cooperate with other molecules present in the matrix, such as its receptor CD44, to form "cable-like" structures that mediate the adhesion of macrophages, monocytes, and T cells (de la Motte et al., 2003)

A recent study in mice revealed that Cemip expression is induced during *Staphylococcus aureus* dermis infection (Dokoshi et al., 2020). Taking advantage of mice lacking *Cemip* gene expression, the researchers demonstrated its central role in hyaluronan digestion during dermis infection and in regulating antimicrobial activity. Interestingly, it seemed that fibroblast-like cells, therefore a cell type with stromal and phenotypical features compatible with MSCs, might be the key producers of Cemip in murine dermis. These findings corroborate with our hypothesis that MSCs can remodel the ECM during infection and CN-NFAT might be instrumental to this scope.

Most trials for GvHD therapy involve the coadministration of MSCs with CN-NFAT inhibitors. For this reason, we harnessed the VIVIT peptide, which inhibits CN-dependent NFAT dephosphorylation without affecting other CN functions (Aramburu, 1999; Noguchi et al., 2004; Yu et al., 2007). We established an MSC line expressing the VIVIT peptide and then analyzed inflammatory cytokine expression. Interestingly, we found that PBMC/$MSC^{VIVIT+}$ cocultures produced lower IL-1β, IL-8, and IL-18 levels compared with PBMC/$MSC^{VIVIT-}$. Thus, although CN-NFAT is not directly involved in MSC cytokine expression, its activity is still important for the interplay between MSCs and immune cells during the antifungal response. One of the reasons for this finding can reside in the correlation between ECM and inflammatory response: the genes regulated by NFAT in MSCs have a relevant role in hyaluronan metabolism and its fragments serve as DAMPs to activate TLRs (Jiang et al., 2005; Taylor et al., 2007a, 2007b). We suggest that a similar process occurs in Ad-MSCs exposed to fungal PAMPs. By our model, Ad-MSCs challenged with zymosan produce antifungal cytokines via NF-κB pathway activation. Zymosan simultaneously induces NFAT pathway activation, which impacts the expression of ECM genes. This latter event promotes DAMPs release and thus helps to attract immune cells during infection, which will contribute to mount the proper immune response. In line with this theory, when we seed PBMCs in decellularized matrices produced by $MSC^{VIVIT+}$ (dVIVIT+), we observed a lower production of IL-8 in response to zymosan, compared to PBMCs seeded on control matrices (dVIVIT-).

In light of these findings, we believe that further studies that dissect how the ECM composition affects immune cell functions will be essential for the future development of successful therapies that harness MSC

immune-suppressive properties. In fact, MSCs have the unique ability to secrete cytokines in response to several types of insult and to produce large amounts of ECM molecules. In our opinion, the latter has been understudied, although it might affect some critical aspects of MSC-based therapy. Specifically, several components of the ECM, including hyaluronan, are also involved in MSC homing to damaged tissue (Corradetti et al., 2017). Dissecting the pathways involved in ECM remodeling, would be beneficial not only in the context of inflammation but also for regenerative medicine, where homing of MSCs to target tissues is highly inefficient and poorly characterized (Ullah et al., 2019). Further studies are now warranted that dissect the molecular mechanisms involved in regulating MSC immune properties, with a focus on their ability to use the ECM to shape the immune response.

### Limitations of the study

In this study we used the PRR ligand zymosan as a model of fungal infection. However, the exact mechanisms of PRR activation and downstream signaling can differ as per the type of fungal pathogen encountered by MSCs, thus potentially resulting in altered signaling.

Using a co-culture of Ad-MSCs and peripheral blood mononuclear cells we showed that selective inhibition of NFAT in Ad-MSCs ($MSC^{VIVIT+}$) modifies the expression of cytokines in the coculture. Taking advantage of this experimental setup, we were able to give insights on CN-NFAT signaling in MSCs. However, in clinical settings, both MSCs and immune cells are exposed to CN-NFAT inhibitors, adding a layer of complexity that goes beyond the scope of our work.

## STAR★METHODS

Detailed methods are provided in the online version of this paper and include the following:

- KEY RESOURCES TABLE
- RESOURCE AVAILABILITY
  - Lead Contact
  - Materials availability
  - Data and code availability
- EXPERIMENTAL MODEL AND SUBJECT DETAILS
  - Cells
- METHOD DETAILS
  - MSCs characterization and FACS analysis
  - Luciferase NF-kB reporter: transfection, selection, and luciferase assay
  - VIVIT-GFP (TetOn) line: transfection and selection
  - Plasmid transfection in HEK-293 cells
  - MSC, THP-1, and macrophage stimulation with PAMPs:
  - RNA extraction and quantitative real time PCR
  - RNA sequencing: sample preparation, library construction and analysis
  - Calcium flux analysis
  - Endocytosis imaging
  - Endocytosis FACS
  - pHrodo-zymosan FACS analysis
  - Protein extraction and Western blotting
  - TRANSAM NF-κB p65
  - IL-6 and IL-8 protein expression in MSC supernatants
  - PBMCs isolation
  - Cytokine expression in co-culture cell supernatants
  - Immunofluorescence staining
  - Decellularization and recellularization with PBMCs
- QUANTIFICATION AND STATISTICAL ANALYSIS

## SUPPLEMENTAL INFORMATION

Supplemental information can be found online at https://doi.org/10.1016/j.isci.2021.102683.

## ACKNOWLEDGMENTS

This study was supported by the European Social Fund and European Regional Development Fund—Project MAGNET (grant no. CZ.02.1.01/0.0/0.0/15_003/0000492) and ENOCH (CZ.02.1.01/0.0/0.0/16_019/0000868); the European Regional Development Fund in frame of the project Kompetenzzentrum MechanoBiologie (grant no. ATCZ133) in the Interreg V-A Austria – Czech Republic program; the National Program of Sustainability II (MEYS CR) (grant no. LQ1605); and the Ministry of Health of the Czech Republic (grant no. NV18-06-00529) and DRO (Institute of Hematology and Blood Transfusion – UHKT, 00023736). This project also received funding from the European Union's Horizon 2020 Research and Innovation Program under grant agreement No 690901 (NANOSUPREMI). Caruso acknowledges the award of a National Health and Medical Research Council Senior Principal Research Fellowship (GNT1135806). F. Cavalieri acknowledges the award of an Australian Research Council (ARC) Future Fellowship scheme (FT140100873). This work was performed in part at the Materials Characterisation and Fabrication Platform (MCFP) at The University of Melbourne.

The authors would like to thank the technical support team at the Center of Translational Medicine, the CF Genomics of CEITEC supported by the NCMG research infrastructure (LM2015091 funded by MEYS CR) for their support with obtaining scientific data presented in this paper, the Biostatistics Core Facility at FNUSA-ICRC for support in RNA sequencing analysis, and Dr Jessica Tamanini of Insight Editing London for reviewing and editing the manuscript prior to submission.

## AUTHOR CONTRIBUTIONS

Conceptualization: F.T. and J.F.; Methodology: F.T.; Software: M.D.Z.; Validation: F.T. and M.D.Z.; Formal Analysis: F.T. and M.D.Z.; Investigation: F.T., M.D.Z., S.S.J., and K.B.; Data Curation: F.T. and M.D.Z.; Writing – Original Draft: F.T. and J.F.; Writing – Review and Editing: F.T., M.D.Z., J.F., G.F., K.B., S.S.J., F. Cavalieri, F. Caruso, and L.K.; Visualization: F.T. and M.D.Z.; Supervision: J.F.; Projects Administration: J.F.; Funding Acquisition: J.F., G.F, and F. Cavalieri.

## DECLARATION OF INTERESTS

The authors declare no competing interests.

Received: September 2, 2020
Revised: February 18, 2021
Accepted: May 31, 2021
Published: June 25, 2021

## REFERENCES

Aramburu, J. (1999). Affinity-driven peptide selection of an NFAT inhibitor more selective than cyclosporin A. Science *285*, 2129–2133.

Armstrong-James, D., de Boer, L., Bercusson, A., and Shah, A. (2018). From phagocytosis to metaforosis: calcineurin's deadly role in innate processing of fungi. PLoS Pathog. *14*, 1–7.

von Bahr, L., Sundberg, B., Lönnies, L., Sander, B., Karbach, H., Hägglund, H., Ljungman, P., Gustafsson, B., Karlsson, H., Le Blanc, K., et al. (2012). Long-term complications, immunologic effects, and role of passage for outcome in mesenchymal stromal cell therapy. Biol. Blood Marrow Transpl. *18*, 557–564.

Balan, A., Lucchini, G., Schmidt, S., Schneider, A., Tramsen, L., Kuçi, S., Meisel, R., Bader, P., and Lehrnbecher, T. (2014). Mesenchymal stromal cells in the antimicrobial host response of hematopoietic stem cell recipients with graft-versus-host disease - friends or foes. Leukemia *28*, 1941–1948.

Bendickova, K., Tidu, F., and Fric, J. (2017). Calcineurin– NFAT signalling in myeloid leucocytes: new prospects and pitfalls in immunosuppressive therapy. EMBO Mol. Med. *9*, 990–999.

Bendíčková, K., Tidu, F., De Zuani, M., Kohoutková, M.H., Andrejčinová, I., Pompeiano, A., Běláśková, S., Forte, G., Zelante, T., and Frič, J. (2020). Calcineurin inhibitors reduce NFAT-dependent expression of antifungal pentraxin-3 by human monocytes. J. Leukoc. Biol. *107*, 497–508.

Borriello, F., Zanoni, I., and Granucci, F. (2020). Cellular and molecular mechanisms of antifungal innate immunity at epithelial barriers: the role of C-type lectin receptors. Eur. J. Immunol. *50*, 317–325.

Bray, N.L., Pimentel, H., Melsted, P., and Pachter, L. (2016). Near-optimal probabilistic RNA-seq quantification. Nat. Biotechnol. *34*, 525–527.

Brown, G.D., and Gordon, S. (2003). Fungal β-glucans and mammalian immunity. Immunity *19*, 311–315. https://doi.org/10.1016/S1074-7613(03)00233-4.

Cao, M., Wu, Z., Lou, Q., Lu, W., Zhang, J., Li, Q., Zhang, Y., Yao, Y., Zhao, Q., Li, M., et al. (2019). Dectin-1-induced RIPK1 and RIPK3 activation protects host against Candida albicans infection. Cell Death Differ. *26*, 2622–2636. https://doi.org/10.1038/s41418-019-0323-8.

Di Carlo, F.J., and Fiore, J.V. (1958). On the composition of zymosan. Science *127*, 756–757.

Corradetti, B., Taraballi, F., Martinez, J.O., Minardi, S., Basu, N., Bauza, G., Evangelopoulos, M., Powell, S., Corbo, C., and Tasciotti, E. (2017). Hyaluronic acid coatings as a simple and efficient approach to improve MSC homing toward the site of inflammation. Sci. Rep. *7*, 7991.

Day, A.J., and Prestwich, G.D. (2002). Hyaluronan-binding proteins: tying up the giant. J. Biol. Chem. *277*, 4585–4588.

Dokoshi, T., Zhang, L.juan, Li, F., Nakatsuji, T., Butcher, A., Yoshida, H., Shimoda, M., Okada, Y.,

and Gallo, R.L. (2020). Hyaluronan degradation by Cemip regulates host defense against Staphylococcus aureus skin infection. Cell Rep. *30*, 61–68.e4.

Edelstam, G.A.B., Laurent, U.B.G., Lundkvist, R.E., Fraser, J.R.E., and Laurent, T.C. (1992). Concentration and turnover of intraperitoneal hyaluronan during inflammation. Inflammation *16*, 459–469.

Fisher, S.A., Cutler, A., Doree, C., Brunskill, S.J., Stanworth, S.J., Navarrete, C., and Girdlestone, J. (2019). Mesenchymal stromal cells as treatment or prophylaxis for acute or chronic graft-versus-host disease in haematopoietic stem cell transplant (HSCT) recipients with a haematological condition. Cochrane Database Syst. Rev. *2019*.

Fric, J., Zelante, T., Wong, A.Y.W., Mertes, A., Yu, H.-B., and Ricciardi-Castagnoli, P. (2012). NFAT control of innate immunity. Blood *120*, 1380–1389.

Galipeau, J., and Sensébé, L. (2018). Mesenchymal stromal cells: clinical challenges and therapeutic opportunities. Cell Stem Cell *22*, 824–833.

Gantner, B.N., Simmons, R.M., Canavera, S.J., Akira, S., and Underhill, D.M. (2003). Collaborative induction of inflammatory responses by dectin-1 and toll-like receptor 2. J. Exp. Med. *197*, 1107–1117.

Goodridge, H.S., Simmons, R.M., and Underhill, D.M. (2007). Dectin-1 stimulation by Candida albicans yeast or zymosan triggers NFAT activation in macrophages and dendritic cells. J. Immunol. *178*, 3107–3115.

Goodridge, H.S., Wolf, A.J., and Underhill, D.M. (2009). β-glucan recognition by the innate immune system. Immunol. Rev. *230*, 38–50.

Goodridge, H.S., Reyes, C.N., Becker, C.A., Katsumoto, T.R., Ma, J., Wolf, A.J., Bose, N., Chan, A.S.H., Magee, A.S., Danielson, M.E., et al. (2011). Activation of the innate immune receptor Dectin-1 upon formation of a 'phagocytic synapse. Nature *472*, 471–475.

Hashmi, S., Ahmed, M., Murad, M.H., Litzow, M.R., Adams, R.H., Ball, L.M., Prasad, V.K., Kebriaei, P., and Ringden, O. (2016). Survival after mesenchymal stromal cell therapy in steroid-refractory acute graft-versus-host disease: systematic review and meta-analysis. Lancet Haematol. *3*, e45–e52.

Herbst, S., Shah, A., Mazon Moya, M., Marzola, V., Jensen, B., Reed, A., Birrell, M.A., Saijo, S., Mostowy, S., Shaunak, S., et al. (2015). Phagocytosis-dependent activation of a TLR9–BTK –calcineurin–NFAT pathway co-ordinates innate immunity to Aspergillus fumigatus. EMBO Mol. Med. *7*, 240–258.

Herre, J., Marshall, A.S.J., Caron, E., Edwards, A.D., Williams, D.L., Schweighoffer, E., Tybulewicz, V., Reis, C., Gordon, S., & Brown, G.D. (2004). Dectin-1 uses novel mechanisms for yeast phagocytosis in macrophages. 104, 4038–4046. https://doi.org/10.1182/blood-2004-03-1140.

Hwa Cho, H., Bae, Y.C., and Jung, J.S. (2006). Role of toll-like receptors on human adipose-derived stromal cells. Stem Cells *24*, 2744–2752.

Imbert, S., Bresler, P., Boissonnas, A., Gauthier, L., Souchet, L., Uzunov, M., Leblond, V., Mazier, D., Nguyen, S., and Fekkar, A. (2016). Calcineurin inhibitors impair neutrophil activity against Aspergillus fumigatus in allogeneic hematopoietic stem cell transplant recipients. J. Allergy Clin. Immunol. *138*, 860–868.

Ji, J., Zhang, D., Wei, W., Shen, B., Zhang, Y., Wang, Y., Tang, Z., Ni, N., Sun, H., Liu, J., et al. (2018). Decellularized matrix of adipose-derived mesenchymal stromal cells enhanced retinal progenitor cell proliferation via the Akt/Erk pathway and neuronal differentiation. Cytotherapy *20*, 74–86.

Jiang, D., Liang, J., Fan, J., Yu, S., Chen, S., Luo, Y., Prestwich, G.D., Mascarenhas, M.M., Garg, H.G., Quinn, D.A., et al. (2005). Regulation of lung injury and repair by Toll-like receptors and hyaluronan. Nat. Med. *11*, 1173–1179.

Jiang, D., Liang, J., and Noble, P.W. (2007). Hyaluronan in tissue injury and repair. Annu. Rev. Cell Dev. Biol. *23*, 435–461.

Kerrigan, A.M., and Brown, G.D. (2010). Syk-coupled C-type lectin receptors that mediate cellular activation via single tyrosine based activation motifs. Immunol. Rev. *234*, 335–352.

Kim, Y.H., Jin, H.J., Heo, J., Ju, H., Lee, H.Y., Kim, S., Lee, S., Lim, J., Jeong, S.Y., Kwon, J.H., et al. (2018). Small hypoxia-primed mesenchymal stem cells attenuate graft-versus-host disease. Leukemia *32*, 2672–2684.

Koldehoff, M., and Zakrzewski, J.L. (2005). Modern management of respiratory failure due to pulmonary mycoses following allogeneic hematopoietic stem-cell transplantation. Am. J. Hematol. *79*, 158–163. https://doi.org/10.1002/ajh.20361.

Lazarus, H.M., Koc, O.N., Devine, S.M., Curtin, P., Maziarz, R.T., Holland, H.K., Shpall, E.J., McCarthy, P., Atkinson, K., Cooper, B.W., et al. (2005). Cotransplantation of HLA-identical sibling culture-expanded mesenchymal stem cells and hematopoietic stem cells in hematologic malignancy patients. Biol. Blood Marrow Transpl. *11*, 389–398.

Luz-Crawford, P., Kurte, M., Bravo-Alegría, J., Contreras, R., Nova-Lamperti, E., Tejedor, G., Noël, D., Jorgensen, C., Figueroa, F., Djouad, F., et al. (2013). Mesenchymal stem cells generate a CD4+CD25+Foxp3 + regulatory T cell population during the differentiation process of Th1 and Th17 cells. Stem Cell Res. Ther. *4*, 65.

Mahmoudifar, N., and Doran, P.M. (2015). Mesenchymal stem cells derived from human adipose tissue. In Methods in Molecular Biology, *1340*, Doran., ed (Humana Press, New York, NY), pp. 53–64.

Medzhitov, R., Preston-Hurlburt, P., and Janeway, C.A. (1997). A human homologue of the Drosophila Toll protein signals activation of adaptive immunity. Nature *388*, 394–397.

Méndez-Ferrer, S., Michurina, T.V., Ferraro, F., Mazloom, A.R., MacArthur, B.D., Lira, S.A., Scadden, D.T., Ma'ayan, A., Enikolopov, G.N., and Frenette, P.S. (2010). Mesenchymal and haematopoietic stem cells form a unique bone marrow niche. Nature *466*, 829–834.

de la Motte, C.A., Hascall, V.C., Drazba, J., Bandyopadhyay, S.K., and Strong, S.A. (2003). Mononuclear leukocytes bind to specific hyaluronan structures on colon mucosal smooth muscle cells treated with polyinosinic acid:polycytidylic acid. Am. J. Pathol. *163*, 121–133.

Muguruma, Y., Yahata, T., Miyatake, H., Sato, T., Uno, T., Itoh, J., Kato, S., Ito, M., Hotta, T., and Ando, K. (2006). Reconstitution of the functional human hematopoietic microenvironment derived from human mesenchymal stem cells in the murine bone marrow compartment. Blood *107*, 1878–1887.

Nagaoka, A., Yoshida, H., Nakamura, S., Morikawa, T., Kawabata, K., Kobayashi, M., Sakai, S., Takahashi, Y., Okada, Y., and Inoue, S. (2015). Regulation of hyaluronan (HA) metabolism mediated by HYBID (Hyaluronan-binding protein involved in HA depolymerization, KIAA1199) and HA synthases in growth factor-stimulated fibroblasts. J. Biol. Chem. *290*, 30910–30923.

Najar, M., Raicevic, G., Boufker, H.I., Kazan, H.F., Bruyn, C. De, Meuleman, N., Bron, D., Toungouz, M., and Lagneaux, L. (2010). Mesenchymal stromal cells use PGE2 to modulate activation and proliferation of lymphocyte subsets: combined comparison of adipose tissue, Wharton's Jelly and bone marrow sources. Cell. Immunol. *264*, 171–179.

Najar, M., Fayyad-Kazan, M., Raicevic, G., Fayyad-Kazan, H., Meuleman, N., Bron, D., and Lagneaux, L. (2018). Advanced glycation End-Products-, C-Type Lectin- and Cysteinyl/leukotriene-receptors in distinct mesenchymal stromal cell populations: differential transcriptional profiles in response to inflammation. Cell J. *20*, 250–258.

Noguchi, H., Matsushita, M., Okitsu, T., Moriwaki, A., Tomizawa, K., Kang, S., Li, S., Kobayashi, N., Matsumoto, S., Tanaka, K., et al. (2004). A new cell-permeable peptide allows successful allogeneic islet transplantation in mice. Nat. Med. *10*, 305–309.

Ritchie, M.E., Phipson, B., Wu, D., Hu, Y., Law, C.W., Shi, W., and Smyth, G.K. (2015). Limma powers differential expression analyses for RNA-sequencing and microarray studies. Nucleic Acids Res. *43*, e47.

Rogers, N.C., Slack, E.C., Edwards, A.D., Nolte, M.A., Schulz, O., Schweighoffer, E., Williams, D.L., Gordon, S., Tybulewicz, V.L., Brown, G.D., et al. (2005). Syk-dependent cytokine induction by dectin-1 reveals a novel pattern recognition pathway for C type lectins. Immunity *22*, 507–517.

Samsonraj, R.M., Raghunath, M., Nurcombe, V., Hui, J.H., van Wijnen, A.J., and Cool, S.M. (2017). Concise review: multifaceted characterization of human mesenchymal stem cells for use in regenerative medicine. Stem Cells Transl. Med. *6*, 2173–2185.

Santus, W., Barresi, S., Mingozzi, F., Broggi, A., Orlandi, I., Stamerra, G., Vai, M., Martorana, A.M., Polissi, A., Köhler, J.R., et al. (2017). Skin infections are eliminated by cooperation of the fibrinolytic and innate immune systems. Sci. Immunol. *2*, eaan2725.

Scheibner, K.A., Lutz, M.A., Boodoo, S., Fenton, M.J., Powell, J.D., and Horton, M.R. (2006). Hyaluronan fragments act as an endogenous

danger signal by engaging TLR2. J. Immunol. *177*, 1272–1281.

Schmidt, S., Tramsen, L., Schneider, A., Schubert, R., Balan, A., Degistirici, Ö., Meisel, R., and Lehrnbecher, T. (2017). Impact of human mesenchymal stromal cells on antifungal host response against Aspergillus fumigatus. Oncotarget *8*, 95495–95503.

Soneson, C., Love, M.I., and Robinson, M.D. (2016). Differential analyses for RNA-seq: transcript-level estimates improve gene-level inferences. F1000Research *4*, 1521.

Sorokin, L. (2010). The impact of the extracellular matrix on inflammation. Nat. Rev. Immunol. *10*, 712–723.

Spaggiari, G.M., Capobianco, A., Abdelrazik, H., Becchetti, F., Mingari, M.C., and Moretta, L. (2008). Mesenchymal stem cells inhibit natural killer-cell proliferation, cytotoxicity, and cytokine production: role of indoleamine 2,3-dioxygenase and prostaglandin E2. Blood *111*, 1327–1333.

Spaggiari, G.M., Abdelrazik, H., Becchetti, F., and Moretta, L. (2009). MSCs inhibit monocyte-derived DC maturation and function by selectively interfering with the generation of immature DCs: central role of MSC-derived prostaglandin E2. Blood *113*, 6576–6583.

Taylor, K.R., Yamasaki, K., Radek, K.A., Di Nardo, A., Goodarzi, H., Golenbock, D., Beutler, B., and Gallo, R.L. (2007a). Recognition of hyaluronan released in sterile injury involves a unique receptor complex dependent on toll-like receptor 4, CD44, and MD-2. J. Biol. Chem. *282*, 18265–18275.

Taylor, P.R., Tsoni, S.V., Willment, J.A., Dennehy, K.M., Rosas, M., Findon, H., Haynes, K., Steele, C., Botto, M., Gordon, S., and Brown, G.D. (2007b). Dectin-1 is required for β-glucan recognition and control of fungal infection. Nat. Immunol. *8*, 31–38. https://doi.org/10.1038/ni1408.

Tesar, B.M., Jiang, D., Liang, J., Palmer, S.M., Noble, P.W., and Goldstein, D.R. (2006). The role of hyaluronan degradation products as innate alloimmune agonists. Am. J. Transpl. *6*, 2622–2635.

Tomchuck, S.L., Zwezdaryk, K.J., Coffelt, S.B., Waterman, R.S., Danka, E.S., and Scandurro, A.B. (2008). Toll-like receptors on human mesenchymal stem cells drive their migration and immunomodulating responses. Stem Cells *26*, 99–107.

Ullah, M., Liu, D.D., and Thakor, A.S. (2019). Mesenchymal stromal cell homing: mechanisms and strategies for improvement. IScience *15*, 421–438.

Wang, S., Zhu, R., Li, H., Li, J., Han, Q., and Zhao, R.C. (2019). Mesenchymal stem cells and immune disorders: from basic science to clinical transition. Front. Med. *13*, 138–151.

Waterman, R.S., Tomchuck, S.L., Henkle, S.L., and Betancourt, A.M. (2010). A new mesenchymal stem cell (MSC) paradigm: polarization into a pro-inflammatory MSC1 or an immunosuppressive MSC2 phenotype. PLoS One *5*, e10088.

Yu, H., Van Berkel, T.J.C., and Biessen, E.A.L. (2007). Therapeutic potential of VIVIT, a selective peptide inhibitor of nuclear factor of activated T cells, in cardiovascular disorders. Cardiovasc. Drug Rev. *25*, 175–187.

Yu, G., Wang, L.G., Han, Y., and He, Q.Y. (2012). ClusterProfiler: an R package for comparing biological themes among gene clusters. Omi. A. J. Integr. Biol. *16*, 284–287.

Yu, L., Xu, Y., Wang, F., Yang, C., Liu, G., and Song, X. (2016). Functional roles of pattern recognition receptors that recognize virus nucleic acids in human adipose-derived mesenchymal stem cells. Biomed. Res. Int. *2016*, 1–16.

Zelante, T., Wong, A.Y.W., Mencarelli, A., Foo, S., Zolezzi, F., Lee, B., Poidinger, M., Ricciardi-Castagnoli, P., and Fric, J. (2017). Impaired calcineurin signaling in myeloid cells results in downregulation of pentraxin-3 and increased susceptibility to aspergillosis. Mucosal Immunol. *10*, 470–480.

Zhao, K., and Liu, Q. (2016). The clinical application of mesenchymal stromal cells in hematopoietic stem cell transplantation. J. Hematol. Oncol. *9*, 46.

## STAR★METHODS

### KEY RESOURCES TABLE

| REAGENT or RESOURCE | SOURCE | IDENTIFIER |
|---|---|---|
| **Antibodies** | | |
| Anti-Dectin-1 antibody | Abcam | Cat# ab140039, RRID:AB_2877055 |
| TLR4 Monoclonal Antibody (76B357.1) | Thermo Fisher Scientific | Cat# MA5-16216, RRID:AB_2537734 |
| Rabbit Anti-NFAT1 Antibody, Unconjugated | Cell Signaling Technology | Cat# 4389, RRID:AB_1950418 |
| Monoclonal Anti-Fibronectin antibody produced in mouse | Sigma-Aldrich | Cat# F7387, RRID:AB_476988 |
| Phospho-Syk (Tyr525/526) Antibody | Cell Signaling Technology | Cat# 2711, RRID:AB_2197215 |
| Syk antibody [SYK-01] | Abcam | Cat# ab3993, RRID:AB_304217 |
| Toll-like Receptor 2 (D7G9Z) Rabbit mAb antibody | Cell Signaling Technology | Cat# 12276, RRID:AB_2797867 |
| CARD9 Antibody | Cell Signaling Technology | Cat# 12416, RRID:AB_2797904 |
| Ras (E8N8L) XP® Rabbit mAb | Cell Signaling Technology | Cat# #67648 |
| MALT1 Antibody | Cell Signaling Technology | Cat# 2494, RRID:AB_2139139 |
| MyD88 (D80F5) Rabbit mAb antibody | Cell Signaling Technology | Cat# 4283, RRID:AB_10547882 |
| Bcl10 (C78F1) Rabbit mAb antibody | Cell Signaling Technology | Cat# 4237, RRID:AB_2228005 |
| TRAF6 (D21G3) Rabbit mAb antibody | Cell Signaling Technology | Cat# 8028, RRID:AB_10858223 |
| GAPDH Loading Control Monoclonal Antibody (GA1R), HRP | Thermo Fisher Scientific | Cat# MA5-15738-HRP, RRID:AB_2537659 |
| Rabbit Anti-beta-Actin Monoclonal Antibody, HRP Conjugated, Clone 13E5 | Cell Signaling Technology | Cat# 5125, RRID:AB_1903890 |
| PE anti-human CD14 antibody | BioLegend | Cat# 325605, RRID:AB_830678 |
| CD73 Monoclonal Antibody (AD2), eFluor 450, eBioscience™, Thermo Fisher Scientific | Thermo Fisher Scientific | Cat# 48-0739-42, RRID:AB_11041811 |
| HLA-DR Monoclonal Antibody (L243), FITC, eBioscience™ | Thermo Fisher Scientific | Cat# 11-9952-42, RRID:AB_2572542 |
| CD105 (Endoglin) Monoclonal Antibody (SN6), eFluor 450, eBioscience™ | Thermo Fisher Scientific | Cat# 48-1057-42, RRID:AB_11219684 |
| FITC anti-human CD90 (Thy1) antibody | BioLegend | Cat# 328108, RRID:AB_893429 |
| PE anti-human CD45 antibody | BioLegend | Cat# 368510, RRID:AB_2566370 |
| PE anti-human CD284 (TLR4) antibody | BioLegend | Cat# 312806, RRID:AB_2205002 |
| Donkey anti-Rabbit IgG (H+L) Highly Cross-Adsorbed Secondary Antibody, Alexa Fluor 488 | Thermo Fisher Scientific | Cat# A-21206, RRID:AB_2535792 |
| Donkey anti-Rabbit IgG (H+L) Highly Cross-Adsorbed Secondary Antibody, Alexa Fluor 555 | Thermo Fisher Scientific | Cat# A-31572, RRID:AB_162543 |
| **Chemicals, peptides, and recombinant proteins** | | |
| Trizol reagent | Invitrogen | Cat# 15596026 |
| Proteinase K | Invitrogen TM | Cat# AM2548 |
| DAPI | Sigma Aldrich (Roche) | Cat# 10236276001 |
| RIPA lysis buffer | Millipore | Cat# 20-188 |
| Puromycin dihydrochloride | SpinChem | Cat# Sc-108071 |
| Pam2CSK4 | InvivoGen | Cat# tlrl-pm2s-1 |

(*Continued on next page*)

*Continued*

| REAGENT or RESOURCE | SOURCE | IDENTIFIER |
|---|---|---|
| Pam3CSK4 | InvivoGen | Cat# tlrl-pms |
| Zymosan | InvivoGen | Cat# tlrl-zyn |
| WGP Dispersible | InvivoGen | Cat# tlrl-wgp |
| ATP | InvivoGen | Cat# tlrl-atpl |
| Piceatannol | InvivoGen | Cat# tlrl-pct |
| FK506 | InvivoGen | Cat# tlrl-fk5 |
| Anti-hDectin-1-IgG | InvivoGen | Cat# mabg-hdect |
| Protease and Phosphatase Inhibitor Cocktail | Sigma Aldrich | Cat# PPC1010 |
| Clarity Western ECL Substrate | Bio Rad | Cat# 1705061 |
| pHrodo™ Green Zymosan Bioparticles™ Conjugate for Phagocytosis | Life Technologies | Cat# P35365 |
| eBioscience™ Calcium Sensor Dye eFluor™ 514 | Thermo Fisher Scientific | Cat# 65-0859 |
| Dextran, Tetramethylrhodamine, 40,000 MW | Thermo Fisher Scientific | Cat# D1842 |
| Dextran, Alexa Fluor™ 488; 10,000 MW | Thermo Fisher Scientific | Cat# D22910 |
| Dextran, Cascade Blue™, 3000 MW | Thermo Fisher Scientific | Cat# D7132 |
| TPCA-1 | Sigma Aldrich | Cat# T1452 |
| Cytochalasin D from Zygosporium mansonii, ≥98% (TLC and HPLC), powder | Sigma Aldrich | Cat# C8273 |
| Lymphoprep | Stemcell Technologies | Cat# 07851 |
| Doxycycline hyclate, ≥98% (HPLC) | Sigma-Aldrich | Cat# D9891 |
| Paraformaldehyde solution 4% in PBS | Santa Cruz Biotechnology | Cat# sc-281692 |
| Ammonium hydroxide solution, 25% in H2O | Fluka | Cat# 44273 |
| **Critical commercial assays** | | |
| Pierce BCA Protein Assay Kit | Thermo Fisher Scientific | Cat# 23225 |
| TransAM NFkB Family | Active Motif | Cat# 43296 |
| Human IL-8/CXCL8 DuoSet ELISA | R&D Systems | Cat# DY814 |
| Human IL-6 DuoSet Elisa | R&D Systems | Cat# DY206 |
| LEGENDplex™ Human Inflammation Panel (13-plex) | BioLegend | Cat# 740809 |
| **Deposited data** | | |
| RNA sequencing | This manuscript | GEO: GSE157981 |
| **Experimental model and Subject details** | | |
| ASC52telo, hTERT immortalized adipose derived Mesenchymal stem cells | ATCC | SCRC-4000 |
| HEK293 | ATCC | CRL-1573 |
| THP-1 | ATCC | TIB-202 |
| hADSC Human Adipose-Derived Stem Cells | Lonza | Catalog# PT-5006 |
| **Oligonucleotides** | | |
| ACTB (Hs01060665_g1) | Thermo Fisher Scientific | Cat# 4331182 |
| GAPDH (Hs02758991_g1) | Thermo Fisher Scientific | Cat# 4331182 |
| IL12B (Hs01011518_m1) | Thermo Fisher Scientific | Cat# 4331182 |
| IL6 (Hs00174131_m1) | Thermo Fisher Scientific | Cat# 4331182 |
| IDO (Hs00984148_m1) | Thermo Fisher Scientific | Cat# 4331182 |
| CXCL8/IL8 (Hs00174103_m1) | Thermo Fisher Scientific | Cat# 4331182 |

(*Continued on next page*)

*Continued*

| REAGENT or RESOURCE | SOURCE | IDENTIFIER |
|---|---|---|
| IL1B (Hs01555410_m1) | Thermo Fisher Scientific | Cat# 4331182 |
| IL-2 (Hs00174114_m1) | Thermo Fisher Scientific | Cat# 4331182 |
| HAS1 (Hs00758053_m1) | Thermo Fisher Scientific | Cat# 4331182 |
| CEMIP (Hs01552114_m1) | Thermo Fisher Scientific | Cat# 4331182 |
| Recombinant DNA | | |
| pLV[TetOn]-Puro-TRE3G>{VIVIT-GFP} | VectorBuilder | VB190423-1074ahm |
| pLV[Exp]-CMV>Tet3G/Hygro | VectorBuilder | VB180123-1018bxq |
| tdTomato-Dectin1A-N-10 | Addgene | Cat#: 58088 |
| Cignal Lenti NFkB Reporter (luc) | Qiagen | CLS-013L |
| Software and algorithms | | |
| ImageJ | Schneider et al., 2012 | https://imagej.nih.gov/ij/; RRID:SCR_003070 |
| Prism v 8.0.1 | GraphPad | https://www.graphpad.com/ ; RRID:SCR_002798 |
| R version 3.6.1 | R Core Team, 2019 | N/A |
| Adobe Illustrator | Adobe | https://www.adobe.com/ ; RRID:SCR_010279 |
| Other | | |
| Mini-PROTEAN® TGX™ Precast Protein Gels | BioRad | Cat# 4561034 |
| µ-Slide VI 0.4 | Ibidi | Cat# 80606 |

## RESOURCE AVAILABILITY

### Lead Contact

Further information and requests for resources and reagents should be directed to and will be fulfilled by the lead contact, Jan Fric (jan.fric@fnusa.cz).

### Materials availability

All unique/stable reagents generated in this study are available from the lead contact with a completed Materials Transfer Agreement.

### Data and code availability

The RNA-sequencing data generated during this study are available at GEO (GEO: GSE157981).

## EXPERIMENTAL MODEL AND SUBJECT DETAILS

### Cells

hTERT immortalized adipose-derived MSC cells (hTERT-MSCs) were obtained from American Type Culture Collection (ATCC, Manassas, Virginia, USA; SCRC-4000)

Poietics human adipose stem cells (Ad-MSC) isolated from three nonobese donors (PT-5006) were purchased from Lonza (Basel, Switzerland). The cells were kept in culture for no longer than five passages.

Both hTERT-MSCs and Ad-MSC were maintained in low-glucose Dulbecco's modified Eagle's medium (DMEM) (1 g/l) with 25mM HEPES without L-glutamine (BioConcept, Basel, Switzerland). To obtain the complete media, low-glucose DMEM was supplemented with 10% fetal bovine serum (FBS), 1% penicillin/streptomycin, and 1% L-glutamine. Cells were incubated at 37°C, 5% $CO_2$, and the medium was changed every other day.

HEK-293 cells were maintained in high-glucose DMEM (4.5 g/l) with 25mM HEPES without L-glutamine (Sigma Aldrich, St. Louis, Missouri). Media was supplemented with 10% FBS, 1% penicillin/streptomycin, and 1% L-glutamine. Cells were incubated at 37°C, 5% $CO_2$, and the medium was changed every other day.

THP-1 monocytic cell line was maintained in RPMI-1640 Medium (Biosera, Nuaillé, France) supplemented with 10% FBS, 1% penicillin/streptomycin.

THP-1-derived macrophages were obtained by stimulating THP-1 with 100nM phorbol 12-myristate 13-acetate (PMA, Sigma Aldrich). After 24 h, medium was changed and cells were allowed to recover for 48 h.

## METHOD DETAILS

### MSCs characterization and FACS analysis

Primary Ad-MSCs at passage four and hTERT-MSCs were harvested using TrypLE Express (Life Technologies, Carlsbad, California, USA). The cells were then stained using the following antibody or antibody cocktails and acquired on FACSCanto II (Becton, Dickinson and Company, Franklin Lakes, NJ, USA):

- Cocktail 1: CD14-PE (HCD14, Biolegend, San Diego, CA, USA) and CD73-eFluor450 (AD2, Thermo Fisher Scientific).
- Cocktail2: HLA-DR FITC (L243, Thermo Fisher Scientific), CD105 eFluor450 (SN6, Thermo Fisher Scientific), CD90-FITC (5E10, Biolegend), and CD45-PE (2D1, Biolegend).
- Antihuman CD284 (TLR4) PE (HTA125, BioLegend).

### Luciferase NF-kB reporter: transfection, selection, and luciferase assay

hTERT-MSCs ($5x10^3$ cells/well) were seeded into a 96-well in media without antibiotics. The cells were transfected with Cignal Lenti NF-kB Reporter (CLS-013L; Qiagen, Hilden, Germany) at MOI = 10. The cells were incubated overnight with the lentiviral particles, before the medium was removed, and the cells were cultivated in complete medium for a further 24 h. Selection was performed in media containing 1 μg/mL puromycin (Santa Cruz Biotechnology, Dallas, Texas, USA). After 5 days of puromycin selection, the hTERT-MSC NF-κB reporter line was tested using LPS as a positive control (data not shown).

hTERT-MSC NF-kB reporter cells were maintained in low-glucose DMEM before subsequent stimulation. The cells were pretreated with 1 μg/mL TPCA-1 (Cell Signaling Technologies, Danvers, Massachusetts, USA) for 30 min and then with 10 μg/mL zymosan (Invivogen, San Diego, California, USA). After 18 h, the cells were lysed using a ONE-Glo Luciferase Assay System (Promega, Sydney, Australia). Luciferase production was detected on a Microplate Luminometer Centro LB 960 (Titertek-Berthold, Pforzheim, Germany).

### VIVIT-GFP (TetOn) line: transfection and selection

The following lentiviral vectors were used to express VIVIT-GFP under the control of the TRE3G promoter: pLV[TetOn]-Puro-TRE3G>{VIVIT-GFP} and pLV[Exp]-CMV>Tet3G/Hygro. These vectors were constructed and packaged by VectorBuilder. The vector ID VB190423-1074ahm and VB180123-1018bxq can be used to retrieve detailed information about the vectors. A GFP-VIVIT plasmid (Addgene plasmid 11106) was used to generate the lentiviral vector and was a gift from Anjana Rao (Aramburu, 1999).

hTERT MSCs were seeded ($5 \times 10^3$/well) in a 96-well plate. The day after the seeding, the cells were transfected with both pLV[TetOn]-Puro-TRE3G>{VIVIT-GFP} and pLV[Exp]-CMV>Tet3G/Hygro (MOI = 10) in complete medium supplemented with 6 μg/mL polybrene (VectorBuilder). After 18 h, the media containing the lentiviral particles were disposed and the transfected cells were selected in media containing 1 μg/mL puromycin and 300 μg/mL hygromycin B (Sigma Aldrich). After 5 days, VIVIT_GFP-MSCs were stimulated with 0.125 μg/mL doxycycline (Sigma Aldrich) to induce VIVIT-GFP expression.

### Plasmid transfection in HEK-293 cells

HEK-293 cells were transfected using Lipofectamine 3000 (Thermo Fisher Scientific, Waltham, Massachusetts, USA). Briefly, cells were seeded to confluence in 100mm petri dish. A pre-incubated mixture containing 1,6mL Opti-MEM media, 12μg tdTomato-Dectin1A-N-10 (gift from Michael Davidson. Addgene plasmid # 58089), 45 μL Lipofectamine 3000 and 30μL P3000 were added to the media. After 18h medium was changed and cells allowed to recover for other 24h.

### MSC, THP-1, and macrophage stimulation with PAMPs:

Cells were seeded into 6-well plates at a density of 8 x $10^5$ cells/ well. Before RNA extraction, cells were stimulated for 6 h with the following ligands: Zymosan 10 μg/ mL (InvivoGen); Pam2CSK4 10 ng/mL (InvivoGen); Pam3CSK4 200 ng/ mL (Invivogen).

### RNA extraction and quantitative real time PCR

Total cellular RNA was extracted from MSCs using TRIzol LS reagent (Thermo Fisher Scientific) according to manufacturer's instructions. The samples were then centrifuged at 14,000 x g for 15 min at 4°C. The upper aqueous phase was collected and mixed with an equal volume of 70% ethanol. The mixture was transferred to an RNAeasy spin column (Qiagen) and purified as per the manufacturer's instructions. The RNA concentration and quality were determined using a Nanodrop 2000 (Agilent, Santa Clara, California, USA). RNA was transcribed into cDNA using the high-capacity cDNA Reverse Transcription Kit (Thermo Fisher Scientific). Real Time PCR (qPCR) was carried out using Taqman Gene Expression Assays and Master Mix (Thermo Fisher Scientific). Finally, RT-qPCR was performed using a LightCycler 480 (Roche, Basel, Switzerland). The Ct values of the genes of interest were normalized to the house-keeping gene GAPDH or ACTB using the ΔCt method.

The following Taqman gene expression assay probes were used:

*ACTB* (Hs01060665_g1)

*GAPDH* (Hs02758991_g1)

*IL12B* (Hs01011518_m1)

*IL6* (Hs00174131_m1)

*IDO* (Hs00984148_m1)

*CXCL8/IL8* (Hs00174103_m1)

*IL1B* (Hs01555410_m1)

*IL-2* (Hs00174114_m1)

*HAS1* (Hs00758053_m1)

*CEMIP* (Hs01552114_m1)

### RNA sequencing: sample preparation, library construction and analysis

Primary human Ad-MSCs from three different donors were used for the experiments after four passages in culture. The cells were seeded to confluence in 10-cm culture dishes. Inhibition with FK506 (0.2 μg/mL) was performed 1 h before stimulation with 10 μg/mL zymosan. After 6 h of zymosan stimulation, RNA extraction was performed as described above. The RNA quality was assessed on Bioanalyzer2100 RNA Nano 6000 chips (Agilent) and samples with RIN >9 were used for sequencing.

An Illumina sequencing library was prepared using the NEBNext Ultra II Directional RNA Library Prep Kit (New England Biolabs, MA, USA) following the manufacturer's instructions. Briefly, total RNA was used for polyA enrichment, then fragmented and transcribed into cDNA. Following universal adapter ligation, the samples were barcoded using NEB dual indexing primers and pooled equimolarly after picogreen quantitation. The sample pool was sequenced using a NextSeq 550 sequencer (Illumina, San Diego, CA) using a 75-cycle high-output cartridge.

Transcript abundances were estimated using kallisto (Bray et al., 2016). The R/Bioconductor package *Tximport* (Soneson et al., 2016) was used to import and summarize transcript-level abundance estimates for gene-level analyses.

Differentially expressed genes (DEGs) were identified using the limma-trend approach (Ritchie et al., 2015) after data filtration, normalization, and patient-specific batch effect removal. DEGs were used as input for gene ontology analyses and gene set enrichment analyses using the R/Bioconductor package *clusterProfiler* (Yu et al., 2012). All the analyses were performed in the R (v3.6.1) environment.

### Calcium flux analysis

Cells were seeded in ibi-treat μ-Slide VI 0.5 Glass Bottom (Ibidi, Munich, Germany) in complete media and incubated overnight. The cells were stained at 37°C for 30 min using Calcium Sensor Dye eFluor™ 514 (eBioscience) 5 μM in DMEM FluoroBrite (Thermo Fisher Scientific) supplemented with 10% FBS, 1% penicillin/streptomycin, and 1% L-glutamine. The excess dye was removed by washing with PBS, and media was added to each channel. Movies were captured under Zeiss LSM 780 confocal microscope equipped with LSM 7 module for live imaging. Each movie recorded 1 frame/s for a total of 60 seconds (~20s before and 40s after injection of the trigger). Analysis of the fluorescence intensity per time in each region of interest (ROI) was performed using ImageJ software.

### Endocytosis imaging

Cells were seeded in ibi-treated μ-Slide VI 0.5 Glass Bottom (Ibidi) in complete media and incubated overnight. The following day, the cells were stimulated for 2 h with Dextran Cascade Blue 3 kDa, Dextran AF488 10 kDa, or Dextran tertamethylrhodamine 40 kDa (Thermo Fisher Scientific) at a concentration of 0.5 mg/mL. Then, the cells were washed twice with PBS and images were captured under a Zeiss LSM 780 confocal microscope.

### Endocytosis FACS

hTERT-MSCs were seeded to confluence into 6-well plates. Before dextran stimulation, control plates were left on ice for 1 h. Cells from both control and experimental groups were stimulated for 2 h with Dextran Cascade Blue 3 kDa, Dextran AF488 10 kDa, or Dextran tetramethylrhodamine 40 kDa. Immediately after, the cells were scraped in PBS supplemented with 1% FBS and 0.5 μM ethylenediaminetetraacetic acid (EDTA) and acquired on a BD FACSCanto™ II cytometer.

### pHrodo-zymosan FACS analysis

hTERT-MSCs were seeded to confluence into 6-well plates. Cells were either pretreated with 1μM cytochalasin D (Sigma Aldrich) for 1 h or left untreated. hTERT-MSCs were then stimulated with pHrodo-zymosan 10μg/mL for 2h. Cells were then scraped in PBS supplemented with 1% FBS and 0.5 μM EDTA and acquired on a BD FACSCanto™ II cytometer.

### Protein extraction and Western blotting

MSCs (~2 x $10^6$) were lysed in 80 μL 1X RIPA buffer (MilliporeSigma, Burlington, Massachusetts, USA) containing 1% protease and phosphatase inhibitor cocktail (Sigma Aldrich). Protein concentrations were determined using a Pierce BCA Protein Assay Kit (Thermo Fisher Scientific). The same amount of protein for each condition was loaded into 10% polyacrylamide gels (Bio-Rad, Hercules, California) prerun at 80 V and then at 100 V. The proteins were transferred to polyvinylidene difluoride membranes using the Trans-Blot Turbo system (Bio Rad). The membranes were blocked with 5% BSA in TBST. All antibody staining solutions were prepared in TBST supplemented with BSA 5%. Staining was performed overnight at 4°C before the membranes were washed and incubated with a secondary antirabbit HRP-conjugated antibody (Sigma Aldrich) at room temperature for 1 h. A GAPDH Loading Control Monoclonal Antibody (GA1R), HRP (Thermo Fisher Scientific), or β-Actin (13E5) Rabbit mAb (HRP Conjugate) #5125 (Cell Signaling Technologies) were used as a loading control. The membranes were then incubated with Clarity™ ECL substrate (Bio Rad) (3–4 min) and chemiluminescence was detected using a ChemiDoc Imaging System (Bio Rad). The signals were quantified using Bio-Rad Lab software.

The following antibodies were used for the analysis:

- Phospho-Syk (Tyr525/526) Antibody #2711 (Cell Signaling Technology)
- Anti-Syk antibody [SYK-01] (ab3993) (Abcam)
- Toll-like Receptor 2 (D7G9Z) Rabbit mAb #12276 (Cell Signaling Technology)

- CARD9 Antibody #12416 (Cell Signaling Technology)
- Ras (E8N8L) XP® Rabbit mAb #67648 (Cell Signaling Technology)
- MALT1 Antibody #2494 (Cell Signaling Technology)
- MyD88 (D80F5) Rabbit mAb #4283 (Cell Signaling Technology)
- Bcl10 (C78F1) Rabbit mAb #4237 (Cell Signaling Technology)
- TRAF6 (D21G3) Rabbit mAb #8028 (Cell Signaling Technology)

### TRANSAM NF-κB p65

MSCs were seeded to confluence into 10-cm culture plates. The cells were left untreated or stimulated for 10 min with 10 μg/mL zymosan before scraping in cold PBS. Nuclear extracts were prepared, and a transcription factor assay for NF-κB p65 was performed using components a TransAM NF-κB Family Kit (Active Motif, Carlsbad, California, USA), as per the manufacturer's instructions. The colorimetric reaction was detected using a Multiskan Go plate reader (Thermo Fisher Scientific). The absorbance was measured at 450 nm, and the reference read was measured at 655 nm.

### IL-6 and IL-8 protein expression in MSC supernatants

Ad-MSCs were stimulated with either TPCA-1 (1 μg/mL) or FK506 (0.2 μg/mL) for 1 h; control cells were left untreated. The cells were then stimulated with 10 μg/mL zymosan for 18 h. The supernatants were collected and immediately frozen. IL-6 and IL-8 expression levels in the cell supernatants were assessed using human IL-6 and human IL-8/CXCL8 DuoSet ELISA kits (R&D Systems, Minneapolis, MN, USA), as per the manufacturer's instructions.

### PBMCs isolation

PBMCs from four healthy donors were isolated from fresh buffy coats (Department of Transfusion and Tissue Medicine of the Brno University Hospital, Brno, Czech Republic) by gradient centrifugation using Lymphoprep (density 1.077 g/ml; STEMCELL Technologies, Vancouver, Canada), as per the manufacturer's recommendations.

### Cytokine expression in co-culture cell supernatants

MSCs-VIVIT (2.5 x $10^4$/well) were seeded in a 24-well plate. MSC-VIVIT+ were stimulated overnight with 0.125 μg/mL DOX. The next day, PBMCs were isolated from four donors as described previously. To achieve a 1:5 ratio of MSC-VIVIT/ PBMCs, 1.25 x $10^5$ PBMCs were added to each well containing VIVIT-MSCs or seeded alone. The cells were either not treated or stimulated with zymosan for 18 h. The cell supernatants were collected and immediately stored at -80°C. Cytokine expression was measured using a Legendplex Multi-Analyte Flow Assay Kit, human inflammation panel 1 (13-plex) for simultaneous quantification of 13 human inflammatory cytokines/chemokines, including IL-1β, IFN-α2, IFN-γ, TNF-α, MCP-1 (CCL2), IL-6, IL-8 (CXCL8), IL-10, IL-12p70, IL-17A, IL-18, IL-23, and IL-33 (BioLegend). Sample preparation and analysis was performed as per the manufacturer's instructions.

### Immunofluorescence staining

Cells were fixed in 4% paraformaldehyde solution (Santa Cruz Biotechnology, Dallas, Texas, USA) and permeabilized with 0.2% Triton X-100 in PBS (AppliChem, Darmstadt, Germany). Then, the samples were blocked with 2.5% BSA in PBS. The following primary antibodies were used overnight at 4°C:

NFAT1 4389s (Cell Signaling Technologies)

TLR4 monoclonal antibody 76B357.1 (Thermo Fisher Scientific)

Anti-dectin-1 antibody ab140039 (Abcam)

The samples were then incubated with the appropriate fluorophore-conjugated secondary antibody for 45 min at RT in the dark. F-actin was labeled with Alexa-Fluor-546- or 647-conjugated phalloidin for 30 min at RT in dark. The nuclei were then counterstained with 4′,6-diamidino-2-phenylindole (DAPI). Images were acquired using a Zeiss LSM 780 confocal microscope.

NFAT1 nuclear intensity was determined using the Intensity Ratio Nuclei Cytoplasm Tool plugin of ImageJ (NIH, USA).

### Decellularization and recellularization with PBMCs

$MSC^{VIVIT+}$ and $MSC^{VIVIT-}$ ($3 \times 10^4$/well) were seeded in a 24-well plates and cultured for 7 days in presence of zymosan (1 μg/mL). Media was changed every other day and, in case of $MSC^{VIVIT+}$, supplemented with doxycycline (0.125 μg/mL). After 7ddays, wells were rinsed with PBS and decellularization was performed using 0.5% Triton + 20 mmol/L $NH_4OH$ for 5 min. Matrices were carefully washed with PBS and recellularized with freshly isolated PBMCs ($1 \times 10^6$/well). Stimulation of PBMCs with zymosan (10 μg/mL) was performed overnight. The supernatants were collected and immediately frozen. IL-8 expression levels in the cell supernatants were assessed using human IL-8/CXCL8 DuoSet ELISA kits (R&D Systems, Minneapolis, MN, USA), as per the manufacturer's instructions.

To verify the integrity of the matrices upon decellularization, some decellularized wells as well as control wells were fixed using 4% paraformaldehyde solution (Santa Cruz Biotechnology), blocked using 2.5% BSA in PBS, and stained with Fibronectin F7387-.2ML (Sigma/Aldrich) and DAPI. Images were then acquired using a fluorescent microscope.

## QUANTIFICATION AND STATISTICAL ANALYSIS

Statistical analyses were performed using GraphPad Prism 6. Unless otherwise indicated, the data represent the means ± SD of at least 3 independent experiments. Statistical tests used for the specific analyses and the number of independent experiments are indicated in each figure legend. * $p \leq 0.05$, ** $p \leq 0.01$, *** $p \leq 0.001$, **** $p \leq 0.0001$. A $p<0.05$ was considered statistically significant. When data were analyzed by repeated-measures one-way ANOVA with the Greenhouse-Geisser correction followed by the Sidak's multiple comparison test, adjusted $p<0.05$ was considered significant.